**Atmospheric
Chemistry
and Physics
Discussions**

A method for evaluating bias in global measurements of CO$_2$ total columns from space

D. Wunch[1], P. O. Wennberg[1], G. C. Toon[1,2], B. J. Connor[3], B. Fisher[2],
G. B. Osterman[2], C. Frankenberg[2], L. Mandrake[2], C. O'Dell[4], P. Ahonen[5],
S. C. Biraud[14], R. Castano[2], N. Cressie[6], D. Crisp[2], N. M. Deutscher[7,8],
A. Eldering[2], M. L. Fisher[14], D. W. T. Griffith[8], M. Gunson[2], P. Heikkinen[5],
G. Keppel-Aleks[1], E. Kyrö[5], R. Lindenmaier[15], R. Macatangay[8], J. Mendonca[15],
J. Messerschmidt[7], C. E. Miller[2], I. Morino[9], J. Notholt[7], F. A. Oyafuso[2],
M. Rettinger[10], J. Robinson[12], C. M. Roehl[1], R. J. Salawitch[11], V. Sherlock[12],
K. Strong[15], R. Sussmann[10], T. Tanaka[9,*], D. R. Thompson[2], O. Uchino[9],
T. Warneke[7], and S. C. Wofsy[13]

[1]California Institute of Technology, Pasadena, CA, USA
[2]Jet Propulsion Laboratory, California Institute of Technology, Pasadena, CA, USA
[3]BC Consulting, Ltd., Alexandra, New Zealand
[4]Colorado State University, Fort Collins, CO, USA
[5]Arctic Research Centre of the Finnish Meteorological Institute, Helsinki, Finland

ACPD

ACOS-GOSAT X$_{CO_2}$ evaluation with TCCON

D. Wunch et al.

Title Page

Abstract	Introduction
Conclusions	References
Tables	Figures

|◀ ▶|
◀ ▶

Back Close

Full Screen / Esc

Printer-friendly Version

Interactive Discussion

[6]Department of Statistics, The Ohio State University, Columbus, OH, USA
[7]University of Bremen, Bremen, Germany
[8]University of Wollongong, Wollongong, NSW, Australia
[9]National Institute for Environmental Studies, Tsukuba, Japan
[10]IMK-IFU, Garmisch-Partenkirchen, Germany
[11]Atmospheric & Oceanic Science, University of Maryland, College Park, MD, USA
[12]National Institute of Water & Atmospheric Research, Wellington, New Zealand
[13]Harvard University, Cambridge, MA, USA
[14]Lawrence Berkeley National Laboratories, Berkeley, CA, USA
[15]Department of Physics, University of Toronto, Toronto, ON, Canada
[*]now at: Japan Aerospace Exploration Agency, Tsukuba, Japan

Correspondence to: D. Wunch (dwunch@gps.caltech.edu)

ACOS-GOSAT X_{CO_2} evaluation with TCCON

D. Wunch et al.

Title Page

Abstract	Introduction
Conclusions	References
Tables	Figures

Back | Close

Full Screen / Esc

Printer-friendly Version

Interactive Discussion

Abstract

We describe a method of evaluating systematic errors in measurements of total column dry-air mole fractions of CO_2 (X_{CO_2}) from space, and we illustrate the method by applying the method to the Atmospheric CO_2 Observations from Space retrievals of the Greenhouse Gases Observing Satellite (ACOS-GOSAT) v2.8 data. The approach exploits the lack of large gradients in X_{CO_2} south of 25° S to identify large-scale offsets and other biases in the ACOS-GOSAT data with several retrieval parameters and errors in instrument calibration. We demonstrate the effectiveness of the method by comparing the ACOS-GOSAT data in the Northern Hemisphere with ground truth provided by the Total Carbon Column Observing Network (TCCON). We use the correlation between free-tropospheric temperature and X_{CO_2} in the Northern Hemisphere to define a dynamically informed coincidence criterion between the ground-based TCCON measurements and the ACOS-GOSAT measurements. We illustrate that this approach provides larger sample sizes, hence giving a more robust comparison than one that simply uses time, latitude and longitude criteria. Our results show that the agreement with the TCCON data improves after accounting for the systematic errors.

1 Introduction

The Greenhouse Gases Observing Satellite (GOSAT) was successfully launched on 23 January 2009, with the goal of measuring total column abundances of CO_2 and CH_4 with unprecedented precision from space (Yokota et al., 2004). GOSAT is a joint venture of the National Institute for Environmental Studies (NIES), the Japanese Space Agency (JAXA) and the Ministry of the Environment (MOE), and carries the Thermal And Near-infrared Sensor for carbon Observation Fourier Transform Spectrometer (TANSO-FTS, Hamazaki et al., 2005), which measures spectra of sunlight reflected from the Earth. Preliminary validation of the NIES/JAXA/MOE GOSAT products is reported in Morino et al. (2011).

The Atmospheric CO_2 Observations from Space (ACOS) project was formed from the Orbiting Carbon Observatory (OCO) project following the OCO launch failure in February 2009. Under an agreement with NIES, JAXA, and the MOE, the ACOS team applied the OCO retrieval algorithm to the GOSAT spectra to compute column-averaged dry-air mole fractions of CO_2 (denoted X_{CO_2}). The ACOS-GOSAT X_{CO_2} data must be independently verified and validated, because they are retrieved using a significantly different algorithm to the NIES/JAXA/MOE retrieval algorithm. In this paper, we discuss the evaluation of the ACOS-GOSAT X_{CO_2} data product by comparing it with more precise and accurate X_{CO_2} measurements from the ground-based Total Carbon Column Observing Network (TCCON, Wunch et al., 2011).

Our technical approach for evaluating the X_{CO_2} product from the ACOS-GOSAT retrievals makes use of the relatively spatially uniform CO_2 in the Southern Hemisphere to identify systematic errors, including large-scale biases and other artifacts caused by the retrieval algorithm or errors in the instrument calibration. Once indentified, these biases are removed and the success of this modification to the data is evaluated through comparisons with the Northern Hemisphere TCCON data. We exploit observed correlations between free-troposphere potential temperature and X_{CO_2} to minimize variability in X_{CO_2} that is dynamic in origin (Keppel-Aleks et al., 2011) when defining coincidence criteria in the Northern Hemisphere. This better defines comparable observations than using a simple geographic constraint.

In Sect. 2, we describe the data products and screening procedures, and we detail our approach to comparing the ACOS-GOSAT X_{CO_2} data product against the TCCON X_{CO_2} measurements in Sect. 3. The techniques are evaluated in Sect. 4, and a discussion and conclusions follow in Sect. 5.

2   Data descriptions

2.1   TCCON data product

The TCCON is a network of calibrated ground-based Fourier transform spectrometers that measure precise and accurate total column amounts of CO_2 and many other species (Wunch et al., 2011). The locations of the stations used in this study are shown in Fig. 1. The TCCON instruments measure the absorption of direct sunlight by trace gas species, and hence they record data only with a direct view of the sun. Because the TCCON instruments are directly solar-viewing, the retrievals of X_{CO_2} are not significantly biased by atmospheric scattering (e.g., aerosols, high cirrus clouds, etc.), nor by surface albedo.

An empirical correction is applied as part of the TCCON retrieval algorithm to remove the spurious airmass-dependent effect caused by spectroscopic inaccuracies (e.g., line widths or relative line strengths). If left uncorrected, these errors would cause the retrieved X_{CO_2} to be around 1 % higher at low airmasses than at high airmasses, creating a spurious diurnal variation that would alias into the seasonal cycle (Deutscher et al., 2010; Wunch et al., 2011). The correction is calculated from daily variations in X_{CO_2} that are directly correlated with airmass (i.e., symmetric about local solar noon), and a single correction factor is applied at all TCCON sites.

The accuracy of the TCCON is determined by comparing the ground-based measurements to integrated profiles of CO_2 measured by WMO-standard instrumentation aboard aircraft (Washenfelder et al., 2006; Deutscher et al., 2010; Wunch et al., 2010; Messerschmidt et al., 2011). The TCCON precision and accuracy in the calibrated X_{CO_2} data presented here are both ∼0.8 ppm (2σ, Wunch et al., 2010).

2.2   ACOS-GOSAT data product

The ACOS-GOSAT data processing algorithm is adapted from the OCO retrieval algorithm (Boesch et al., 2006; Connor et al., 2008; Boesch et al., 2011) and incorporates

modifications required to accurately represent the physics of the GOSAT instrument, such as the instrument line shape and noise model. The inverse method is based on the optimal estimation approach given by Rodgers (2000). The forward model is based on LIDORT (Spurr et al., 2001; Spurr, 2002), and a two-order scattering model to account for polarization, described by Natraj and Spurr (2007). A "low-streams interpolation" scheme, devised by O'Dell (2010), ensures that the scattering calculation is both fast and accurate.

The molecular absorption coefficients for CO_2 (Toth et al., 2008) and O_2 (Long et al., 2010) have been extended to account for line mixing and collision-induced absorption using the results of Hartmann et al. (2009) for CO_2 and of Tran and Hartmann (2008) for O_2. The disk-integrated solar spectrum is based on ground-based measurements from the Kitt Peak Fourier transform spectrometer. All other molecular spectral parameters are taken from HITRAN 2008 (Rothman et al., 2009). Surface pressure is retrieved from the oxygen A-band near 0.76 µm. The CO_2 columns are retrieved from the weak band near 1.61 µm, and the strong band near 2.1 µm. The spectral ranges used in the ACOS algorithm match those of the OCO and future OCO-2 instrument.

2.2.1 ACOS-GOSAT data screening

We use the v2.8 release of the ACOS-GOSAT data, available from the Goddard Data and Information Services Center (GDISC, see note ACOS-GOSAT Data Access), spanning 5 April 2009 through 21 March 2011. These retrievals are pre-screened to include only cloud-free scenes. The ACOS-GOSAT data product includes a "master quality flag" that provides an estimate of confidence in the retrieved X_{CO_2} and its associated a posteriori error. The master quality flag uses filters that are described in the ACOS readme document also available from the GDISC (Savtchenko and Avis, 2010). Here, we apply post-processing filters that are slightly different from those used to derive the master quality flag provided with the data. The filters as applied are listed in Table 1 and are chosen to limit the retrievals to those in which we have the highest confidence. The main differences between the filters applied here and those used to determine the

master quality flag are in the quality of the spectral fit (i.e., reduced χ^2), the allowed deviation of the retrieved surface pressure from the a priori, and a few additional filters as described below.

Retrievals are defined as successful by the master quality flag when they satisfy $\chi^2 < 1.2$. However, the χ^2 values have increased linearly over time, because the time-dependent radiometric calibration owing to a sensitivity degradation of the O_2 A-band channel was not applied to the noise model. To compensate for this, we adjust the cutoff value so that it starts at 1.2 and evolves with a linear increase in time, matching the increase in minimum χ^2. As a result, a similar number of scenes are retained over time.

Data with retrieved surface pressure (P_{surf}) that differs significantly from the ECMWF a priori surface pressure (P_{ECMWF}) are marked as 'bad' in the master quality flag. Data are retained by the master quality flag when the difference between the retrieved and a priori surface pressures:

$$\Delta P \equiv (P_{surf} - P_{ECMWF}) \tag{1}$$

is $0 < \Delta P < 20$ hPa. In this work, scenes are retained that satisfy: $|(\Delta P) - \overline{(\Delta P)}| < 5$ hPa. The global mean value of $\overline{\Delta P}$ is approximately 10.9 hPa.

We apply three additional filters: one to remove the medium-gain scenes, one to remove the glint measurements, and one to remove scenes that contain surface ice or snow. The medium-gain (M-gain) TANSO-FTS mode, which is used over very bright surface scenes (Fig. 2), is known to have ghosting issues caused by mismatched timing delays in the signal chain (Suto and Kuze, 2010). In future releases of the spectra, this ghosting effect will be corrected, but in the meantime, we do not use the M-gain data. Glint measurements are made exclusively over ocean and have different properties than the nadir measurements made over land. The ACOS-GOSAT glint retrieval algorithm requires additional refinement, so glint retrievals are not considered here.

A fraction of the ACOS-GOSAT retrievals exhibit anomalously low values due to the presence of snow- and ice-covered land surfaces. We apply a filter that depends on

the retrieved albedos of the O_2 A-band (A_{AO_2}) and the strong CO_2 band (A_{SCO_2}). We will call this combination of albedos the "blended albedo." The blended albedo was determined from a multivariate linear regression on the data, which was trained on scenes known to have snow or ice conditions at the surface, and correctly characterises
⁵ over 99.9 % of the scenes. Data that are retained satisfy Eq. (2), and their distribution is shown in Fig. 3

$$\text{blended albedo} \equiv 2.4 A_{AO_2} - 1.13 A_{SCO_2} < 1. \tag{2}$$

3 Comparing satellite-based X_{CO_2} with ground-based TCCON measurements

Observations and models of surface, partial and total column amounts of CO_2 in the
¹⁰ Southern Hemisphere show low seasonal and geographic variability compared with the Northern Hemisphere. Observations from the global network of in situ atmospheric CO_2 measurements show that surface CO_2 concentrations at latitudes between 25° S and 55° S have a small seasonal cycle (~1 ppm peak-to-peak), and small geographic gradients (GLOBALVIEW-CO_2, 2006). Olsen and Randerson (2004) predicted such
¹⁵ uniformity in modeling the total columns of CO_2 in the Southern Hemisphere. Measurements of CO_2 profiles from the recent Hiaper Pole-to-Pole Observations (HIPPO) campaign by Wofsy et al. (2011) also show that the Southern Hemisphere CO_2 field does not vary by more than 1.6 ppm south of 25° S. Figure 4 shows the HIPPO CO_2 data centred on the Pacific Ocean.
²⁰ There are two TCCON stations located south of 25° S: Wollongong, Australia (34° S) and Lauder, New Zealand (45° S). Wollongong is located on the Australian eastern coast, on the outskirts of a small urban centre, located about 100 km south of Sydney. Lauder is located on New Zealand's south island and predominantly samples clean maritime air. The Lauder site has a seasonal cycle in X_{CO_2} with a small peak-to-peak
²⁵ amplitude of about 0.6 ppm (Fig. 5). The measurements over Wollongong are affected by local pollutants which can increase the seasonal cycle of X_{CO_2} over Wollongong to

Full Screen / Esc

Printer-friendly Version

Interactive Discussion

~2 ppm peak-to-peak, but this is variable from year to year. When the effect from the pollution is accounted for, the background seasonal cycle is reduced to ~1 ppm peak-to-peak. The Lauder X_{CO_2} time series is the longest in the Southern Hemisphere, and has a secular increase of 1.89 ppm yr^{-1} since 2004, which is in good agreement with the global mean secular increase of about 2 ppm yr^{-1} (with a year-to-year variability of 0.3 ppm yr^{-1}, 1σ) from the GLOBALVIEW surface in situ flask network over the same time period (Conway and Tans, 2011).

Consistent with HIPPO, TCCON, and GLOBALVIEW, we assume that the Southern Hemisphere poleward of 25° S has a small seasonal cycle in X_{CO_2} of ~0.6 ppm (peak-to-peak), has no geographic gradients and a secular increase of 1.89 ppm yr^{-1}. The ACOS-GOSAT data between 25° S and 55° S show spatial and temporal variations that substantially exceed this constraint. We assume this additional variance is spurious and look for empirical correlations of X_{CO_2} with retrieval or instrument parameters. We assume that these correlations represent systematic errors that exist globally. After accounting for these biases, we evaluate the ACOS-GOSAT X_{CO_2} data against TCCON data globally.

3.1 Bias determination from the Southern Hemisphere

The filtering described in Sect. 2.2.1 removes spectra recorded under atmospheric conditions that are not yet modeled well in the ACOS retrieval (e.g., surface ice). However, these filters do not remove all systematic errors in the treatment of the instrument calibration, spectroscopy, measurement geometry, or other features. This section discusses the identification of these biases.

Known deficiencies in the implementation of the spectroscopic line shape of the O_2 A-band and the strong CO_2 bands cause systematic biases in the retrieved X_{CO_2}. In the absence of an improved line shape model (currently under development), the biases can either be removed after the retrieval by calibrating against known X_{CO_2} values, or by scaling the cross-sections before the retrieval. The method that will be employed

by the ACOS team in a future version of the algorithm is to scale the cross-sections of the O_2 A-band in order to retrieve the known column of atmospheric O_2, and to ensure that the spectroscopic parameters describing the strong CO_2 band result in a retrieval that yields the same column amount as the weak CO_2 band for the same atmospheric conditions. The v2.8 algorithm does not use scaled cross-sections, so here we perform an initial "calibration" of the ACOS-GOSAT X_{CO_2} data using Southern Hemisphere TC-CON data. The mean ratio between the summertime (December, January, February) Lauder TCCON data and the corresponding ACOS-GOSAT data within $\pm 5°$ latitude of Lauder is $\sim 2\%$. We have thus corrected this bias globally by dividing all ACOS-GOSAT data by 0.982 (Fig. 6). Much of this bias is due to the retrieved surface pressure offset (ΔP), described in Sect. 2.2.1.

From the v2.8 release of the ACOS-GOSAT product, we select the most significant parameters that reduce the variance of the X_{CO_2} anomalies in the Southern Hemisphere south of $25°$ S. The anomalies are computed by subtracting a $1.89\,\mathrm{ppm\,yr^{-1}}$ slope with a seasonal cycle derived from the Baring Head, New Zealand GLOBALVIEW seasonal climatology (GLOBALVIEW-CO_2, 2006) from the ACOS-GOSAT data between $25°$ S and $55°$ S. Because the GLOBALVIEW data replicate the in situ seasonal cycle at the surface and not the column seasonal cycle, we have applied a time lag of 6 weeks and have reduced the amplitude by multiplying by 0.65 to best match the seasonal cycles at Lauder and Wollongong (Fig. 5).

In order of importance, the most significant parameters correlated with this spurious variability in the retrieved X_{CO_2} are the blended albedo (defined in Eq. 2), ΔP (defined in Eq. 1), airmass (described in Eq. 3 below), and the continuum level of the O_2 A-band spectral radiance (called "signal_o2" in the v2.8 data files). The airmass is approximated by

$$\text{airmass} = 1/\cos(\text{solar zenith angle}) + 1/\cos(\text{observing angle}), \qquad (3)$$

where solar zenith angle is the angle of the sun, and observing angle is the off-nadir viewing angle of the instrument. (These parameters are labeled "sounding_solar_zenith,"

and "sounding_zenith," respectively, in the v2.8 data files.)

A multivariate linear regression on the blended albedo, ΔP (in hPa), the airmass, and the signal_o2 (in $W\,cm^{-2}\,sr^{-1}\,(cm^{-1})^{-1}$) suggests that the following modification to the retrieved X_{CO_2} (in ppm) partially removes the biases:

$$X_{CO_2}^{modified} = \frac{X_{CO_2}^{retrieved}}{C_0} - C_1(\text{blended\_albedo} - \overline{\text{blended\_albedo}}) - C_2(\Delta P - \overline{\Delta P})$$
$$- C_3(\text{airmass} - \overline{\text{airmass}}) - C_4\left(\text{signal\_o2} \times 10^7 - \overline{\text{signal\_o2} \times 10^7}\right) \qquad (4)$$

where the coefficients are $C_0 = 0.982$, $C_1 = 10.5$ ppm/units of blended albedo, $C_2 = -0.15$ ppm hPa^{-1}, $C_3 = -2.0$ ppm/airmass and $C_4 = -0.25$ ppm/ $(10^7 W\,cm^{-2}\,sr^{-1}\,(cm^{-1})^{-1})$. Subtracting off the mean values, which are listed in Table 2, minimizes the overall change in X_{CO_2}. Scatter plots of the simultaneous regressions are shown in Fig. 7. If only the secular increase is removed from the Southern Hemisphere data to produce the anomalies (i.e., if we do not include the small seasonal cycle), the regression coefficients agree within two bootstrapped standard errors with the coefficients in Eq. (4). Further, if we apply a -1 ppm gradient between $25°$ S and $55°$ S to approximate the HIPPO observations, the coefficients again agree, within two bootstrapped standard errors (see Table 2). The bootstrapping technique is described by, for example, Efron and Gong (1983).

These basis functions (blended albedo, ΔP, airmass, signal_o2) are not orthogonal, and other parameters may be used to accomplish a similar reduction in the variability of retrieved X_{CO_2}. Errors in aerosol and cloud characterization or identification can affect the retrieved albedos and hence the blended albedo parameter, and they can also affect the retrieved path length and ΔP. The relationship of X_{CO_2} to blended albedo is also seen in retrievals on simulated data, suggesting that at least part of this relationship is caused by the retrieval algorithm. The simulated data are derived from an orbit simulator developed by O'Brien et al. (2009) as a test bed for the OCO algorithm. The simulator contains no errors due to spectroscopy or the instrument, and

Title Page

Abstract | Introduction

Conclusions | References

Tables | Figures

◄ | ►|

◄ | ►

Back | Close

Full Screen / Esc

Printer-friendly Version

Interactive Discussion

hence provides an excellent test of the retrieval algorithm.

Outside the simulator, there are several known causes of systematic effects on the retrievals. First, errors in the spectroscopy can produce spurious airmass dependences as well as global biases (e.g., Yang et al., 2005; Hartmann et al., 2009; Deutscher et al., 2010; Wunch et al., 2011) and can affect the pressure retrieval (e.g., ΔP). Another error source is from nonlinearities in the instrument signal chain that can manifest themselves as zero-level offsets in the O_2 A-band. Zero-level offsets in a Fourier transform spectrometer depend strongly on the signal at zero path difference, and hence on the average signal level of the spectrum (Abrams et al., 1994). As a proxy for the average signal level, which is not available in the public v2.8 data, we use the continuum level radiance ("signal_o2"), which is highly correlated with the average signal level ($r^2 = 0.994$). Disentangling biases associated with the spectral continuum level from the airmass is difficult, because they are strongly anti-correlated.

Future releases of spectra from the GOSAT team will account for the zero-level offset explicitly, either as in Butz et al. (2011), or, preferably, in the measured radiances in the interferograms, prior to the Fourier transform, once the underlying instrumental cause is properly quantified. With these corrections, we expect that the systematic error on X_{CO_2} caused by the signal_o2 dependence will be significantly reduced.

Finally, there is a photosynthetic fluorescence signal in the O_2 A-band (Frankenberg et al., 2011; Joiner et al., 2011). Its potential impact on the retrieval of scattering properties in the A-band is described by Frankenberg et al. (2011) and makes use of the Fraunhofer lines near the O_2 A-band. This effect is currently ignored in the X_{CO_2} retrievals and can give rise to systematic biases. Over photosynthetically active regions of the globe, the vegetation fluoresces, adding a broad-band signal throughout the O_2 A-band. If this additional signal is not included in the forward model, the measured O_2 lines appear shallower than expected, and the retrieved X_{CO_2} will be incorrect (too high), with a seasonal cycle from the vegetation fluorescence imposed on top of the true X_{CO_2} seasonal cycle that is of interest here. The effects of fluorescence will be retrieved and the fluorescence data will be available in a future release of the

Title Page

Abstract | Introduction

Conclusions | References

Tables | Figures

◄ | ►

◄ | ►

Back | Close

Full Screen / Esc

Printer-friendly Version

Interactive Discussion

ACOS-GOSAT data.

In applying Eq. (4) to the global dataset, we assume that the dependencies of ΔX_{CO_2} on the parameters are linear, and can be reasonably extrapolated to values found outside the range in the Southern Hemisphere. The Northern Hemisphere and Southern Hemisphere have similar distributions of ΔP, blended albedo and signal_o2, but the Northern Hemisphere data contain a larger range of airmasses. In the Southern Hemisphere, 99 % of the data poleward of 25° S have sampled airmasses between 2 and 3.3. In the Northern Hemisphere, 99 % of the data poleward of 25° N have sampled airmasses between 2 and 5.1. Any nonlinearity in the airmass-ΔX_{CO_2} relationship will result in a residual airmass dependency in the modified Northern Hemisphere data.

3.2 Applying averaging kernels

To compare two X_{CO_2} observations properly, the retrievals must be computed about a common a priori profile, and the effect of smoothing must be taken into account by applying the averaging kernels (Rodgers and Connor, 2003). Since the v2.8 ACOS and TCCON retrievals were computed using different a priori profiles, we must adjust the retrieved X_{CO_2} values accordingly (see Sect. A for the mathematical details). To test the effect of this adjustment and of the smoothing, we select retrievals within ±0.5° latitude and ±1° longitude of the Lamont TCCON site. We cannot test the effects of the averaging kernels globally because this requires an estimate of the real atmospheric variability everywhere, which is unknown. We can generate an estimate of the atmospheric variability over Lamont, however, by using the bi-weekly low-altitude (0–5 km) aircraft measurements of CO_2 profiles over the Lamont TCCON station (Fig. 8) and the surface CO_2 measurements from the co-located tall tower when they were available. Each profile was extrapolated up to 5500 m and down to the surface altitude (315 m) from the nearest available data point, resulting in 177 profiles recorded between January 2006 and November 2009. In order to compute the weekly variance over several years of observations, a secular increase of 1.89 ppm yr^{-1} was subtracted from all altitudes of the profiles. Next, we adjust the ACOS-GOSAT values to the ensemble profile,

which we assume to be the TCCON a priori profile. This results in an adjustment to the ACOS-GOSAT X_{CO_2} that is seasonal, with an amplitude of about 0.5 ppm. It may also have a small secular decrease of about 0.1 ppm yr^{-1} as well, which could be due to the differences in the secular increases in the ACOS-GOSAT and TCCON a priori profiles. The ACOS X_{CO_2} values are adjusted downward in the winter, and upward in the summer, which has the effect of reducing the overall seasonal cycle of the ACOS-GOSAT retrieval (Fig. 9). The adjustment at Lamont has a seasonal cycle because the ACOS-GOSAT a priori profile does not contain a seasonal cycle, whereas the real atmosphere does (Fig. 1). This implies that the adjustment to the ACOS-GOSAT data will be latitude-dependent, with the smallest adjustments in the Southern Hemisphere, and the largest adjustments at the latitude of the Boreal forests (i.e., around 50–65° N), where the seasonal cycle has the largest amplitude.

The smoothing error (defined in the caption and given by the red curve in Fig. 9) is about 0.6 ppm, which is smaller than the sum of the variances of the ACOS-GOSAT X_{CO_2} and the TCCON X_{CO_2} (~1.5 ppm) but not negligibly so. The effect of smoothing the TCCON data using the ACOS-GOSAT averaging kernel results in a bias of about 0.6 ppm with no significant seasonal cycle or airmass dependence (the yellow curve in Fig. 9).

Applying the averaging kernels in a globally consistent manner is not possible without a global estimate of atmospheric variability. However, we can draw two important conclusions from the Lamont test:

1. There is a seasonal cycle induced by the adjustment of the ACOS-GOSAT data to the TCCON a priori profile. It has an amplitude of about 0.5 ppm at Lamont. The amplitude of the adjustment will likely have a latitude dependence.

2. There is a bias of about 0.6 ppm induced by smoothing the TCCON profile with the ACOS-GOSAT averaging kernel at Lamont.

The TCCON a priori profile is being evaluated for a future version of the ACOS-GOSAT algorithm, which would make the adjustment step unnecessary.

Our correction scheme described by Eq. (4) should significantly reduce airmass dependencies caused by global error terms (e.g., spectroscopic errors) and the overall bias. This will not be perfect, of course, and the results will likely contain a latitude-dependent seasonal bias. Once the TCCON priors are used for the ACOS-GOSAT retrievals, the discrepancies caused by the a priori profiles will be eliminated, leaving us only to consider the smoothing error. For the remainder of this paper, only the adjustments in Eq. (4) are applied.

4 Comparisons in the Northern Hemisphere

The first step in evaluating the Northern Hemisphere seasonal cycles from the ACOS-GOSAT data before and after applying Eq. (4) is to inspect the retrieved values in latitude bands corresponding to TCCON sites. Figure 10 shows latitude bands containing the 11 TCCON sites used in this study. The Tsukuba TCCON data were adjusted up by 1.32 ppm in this analysis, due to a known instrumental bias that has been characterized through aircraft calibration campaigns (Tanaka et al., 2011).

The seasonal cycle shape, after applying Eq. (4) to the ACOS-GOSAT data, is generally improved over the data that has only the global bias removed (0.982). Site-by-site investigations require stricter coincidence criteria. However, criteria based on tight geographic and temporal constraints result in few coincidences at higher latitude sites, because the surface is covered in snow, or it is often cloudy.

We can loosen geographic and temporal constraints on the coincidence criteria if we exploit the relationship between the free-tropospheric potential temperature and variability in X_{CO_2} in the Northern Hemisphere (Fig. 11). Keppel-Aleks et al. (2011) detail the use of the potential temperature coordinate as a proxy for equivalent latitude for CO_2 gradients in the Northern Hemisphere. We use the mid-tropospheric temperature field at 700 hPa, T_{700} (which is directly proportional to the potential temperature at 700 hPa for the range of temperatures of interest here), to allow a significantly broader comparison between TCCON and ACOS-GOSAT than could be found

using only geographic coincidence. The pressure (700 hPa) is arbitrary, and any mid-tropospheric pressure would do. Choosing 700 hPa is convenient, however, because the NCEP/NCAR analysis product is provided on a 700 hPa grid level (Kalnay et al., 1996), and the NCEP/NCAR data provide the a priori atmospheric information to the TCCON retrieval algorithm. A Northern Hemisphere map of the NCEP/NCAR T_{700} field for 10 days in August 2010 is shown in Fig. 12.

For our coincidence criteria, we find GOSAT measurements within 10 days, latitudes within ±10° and longitudes within ±30° of the TCCON site, for which T_{700} is ±2 K of the value over the TCCON site. The longitude limits for Tsukuba are set to be ±10° because we do not wish to inadvertently over-weight the measurements over China. The possible locations of the coincidences for each TCCON site, given the latitude, longitude, and T_{700} of each site, are overlaid on the map in Fig. 12. This set of criteria results in many more coincident measurements over the higher latitude sites. For example, over Park Falls, the T_{700} criterion results in 10 times more coincident measurements than using a geographic constraint of ±0.5° latitude and ±1.5° longitude.

These criteria are applied to generate Fig. 13, which shows the site-by-site comparisons in the Northern Hemisphere. The correlations between TCCON and ACOS-GOSAT are shown in Fig. 14. All slopes are quoted as $x \pm y$, where x is the best fit slope and y is twice the standard error on the best fit, calculated using the method outlined in York et al. (2004). The slope is significantly improved after applying Eq. (4) (compare the left and middle panels of Fig. 14). Selecting a T_{700} coincidence criterion also improves the correlation coefficient (r^2) over a simple latitude/longitude/time coincidence (compare the middle and right panels of Fig. 14). When using a T_{700} constraint of ±1 K (instead of ±2 K), the r^2 decreases, and the comparison dataset diminishes significantly (10 % loss in data over Park Falls, and 25 % loss in data over Tsukuba). A constraint of ±3 K shows no reduction in r^2, but also no significant gain in coincident measurements, as the geographic constraints become dominant.

The correlation slope between the ACOS-GOSAT and TCCON data is not unity within the uncertainty: it is 0.86 ± 0.07 with an r^2 of 0.80. This difference from unity is

partially due to a time-dependent difference in X_{CO_2} between the TCCON data and the ACOS-GOSAT data. This could imply that there is a residual radiometric calibration error (due to degradation of the mirrors or other optical components) or another time-dependent effect. A residual airmass-dependent error remains, especially at very high airmasses, and indeed the assumed linear regression reduces the agreement at very high airmasses. This is clear in the Eureka and Sodankylä time series and, to a lesser extent, in the Białystok time series. Limiting the correlation plot to airmasses ≤3.3 improves the r^2 and increases the slope (to 0.85 and 0.89 ± 0.08, respectively). The additional airmass-dependent errors may be reduced by adjusting the ACOS-GOSAT retrieval to the TCCON a priori profile and accounting for the photosynthetic fluorescence signal. OCO-2's target mode will allow for a determination of the airmass dependence globally.

Even after modification of the ACOS-GOSAT data by Eq. (4), the ACOS-GOSAT noise is too large to see significant interannual X_{CO_2} drawdown differences. Figure 11 shows the relationship between ΔX_{CO_2} and T_{700} in the Northern Hemisphere for 2009 and 2010. Although the range of potential temperatures sampled at the TCCON sites differs substantially between 2009 and 2010 (because the Eureka and Sodankylä sites were not yet recording X_{CO_2} data), all TCCON sites operating in both 2009 and 2010 show a stronger ΔX_{CO_2} drawdown (2–3 ppm) in August 2009 than in 2010. This interannual difference is indistiguishable in the ACOS-GOSAT data, as it is within its noise (plotted as 1σ error bars). As further improvements to the ACOS algorithms are implemented, the noise should reduce, and we anticipate that these important interannual features will become separable from the noise.

5 Discussion and conclusions

Estimating sources of bias in satellite observations is essential if the data are to be used to infer surface fluxes. The ACOS retrievals of X_{CO_2} from the GOSAT TANSO-FTS instrument contain global and regional systematic errors. We have demonstrated

that bias between the ACOS-GOSAT retrieval of X_{CO_2} data and TCCON X_{CO_2} is significantly reduced if a set of modifications determined from the Southern Hemisphere data is applied globally. After applying the modifications to the data described by Eq. (4), the comparisons of ACOS-GOSAT X_{CO_2} to TCCON are significantly improved but remain
5   imperfect and show both residual time and airmass dependences. Future versions of the ACOS-GOSAT data will include an updated radiometric calibration, a fluorescence correction and a nonlinearity correction, and will use a seasonally and latitudinally varying a priori profile, all of which should improve the retrievals.

One underlying assumption in this work has been that the X_{CO_2} gradients in the
10 Southern Hemisphere are small. We expect that as the quality of the satellite data improves, this assumption will become less valid. In future work, using assimilations of Southern Hemisphere CO_2 (e.g., CarbonTracker, described by Peters et al., 2007) and the Southern Hemisphere TCCON sites could provide a more robust estimate of the true Southern Hemisphere X_{CO_2} fields. A second important assumption we have
15 made is that the spurious variability in the Northern Hemisphere is caused by the same retrieval or instrument parameters that cause the spurious variability in the Southern Hemisphere. Anywhere that this assumption is invalid will lead to residual variability and bias in the Northern Hemisphere.

When turning to comparisons of ACOS-GOSAT X_{CO_2} with TCCON in the Northern
20 Hemisphere, coincidence criteria that include the temperature at 700 hPa, which serves as a tracer of dynamically-driven variability in X_{CO_2}, allow for a broader comparison with larger sample sizes. The ACOS-GOSAT noise in v2.8 is still too large to distinguish interannual variability in the Northern Hemisphere seasonal cycles in 2009 and 2010, but we anticipate that future versions of the ACOS algorithm will be able to clearly
25 distinguish the two years.

The methods outlined in this paper: using the Southern Hemisphere to define modifications to remove spurious variability, and using the temperature at 700 hPa to define coincidence criteria in the Northern Hemisphere, are readily applicable to other satellite instruments observing X_{CO_2}, such as the Scanning Imaging Absorption Spectrometer

for Atmospheric Chartography (SCIAMACHY Burrows et al., 1995). These methods are directly applicable to the future OCO-2 retrieval algorithm, and will form the basis for initial evaluations of the OCO-2 data.

Appendix A

The effect of averaging kernels

The averaging kernels and a priori profiles for the ACOS-GOSAT retrievals over Lamont and the TCCON FTS retrievals are shown in Figs. 1 and 2. According to Rodgers and Connor (2003), to compare retrieval results from two different instruments with differing viewing geometries, retrieval algorithms, a priori profiles (x_a) and averaging kernels (**A**), an "ensemble" profile (x_c) and covariance matrix (S_c) should be selected, which represent the mean and variability of the ensemble of true atmospheric profiles over which the comparison is to be made. That is, in order to compare retrieved values $\hat{x}_i$ from the i-th instrument, the equations, traditionally written as

$$\hat{x}_i - x_{ai} = \mathbf{A}_i(x - x_{ai}) + \boldsymbol{\epsilon}_{xi} \tag{A1}$$

with measurement error $\boldsymbol{\epsilon}_{xi}$, should be "adjusted" to a common comparison ensemble, x_c, by adding $(\mathbf{A}_i - \mathbf{I})(x_{ai} - x_c)$ to both sides of the equation, giving our new, adjusted equations:

$$\hat{x}'_i - x_c = \mathbf{A}_i(x - x_c) + \boldsymbol{\epsilon}_{xi} \tag{A2}$$

where $\hat{x}'_i$ is the "adjusted" $\hat{x}$, and **I** is the identity matrix:

$$\hat{x}'_i \equiv \hat{x}_i + (\mathbf{A}_i - \mathbf{I})(x_{ai} - x_c) \tag{A3}$$

We are interested in comparing the dry-air mole fractions (DMFs, X_{CO_2}) in ppm, and not the profiles of CO_2. The X_{CO_2} are computed by dividing the total column abundances

of CO_2 by the column of dry air.

$$X_{CO_2} = \frac{\text{column } CO_2}{\text{column dry air}} \tag{A4}$$

The column of dry air can be computed in two ways: directly using a measurement of the O_2 column, and using the surface pressure (P_{surf}) corrected for the H_2O column:

$$\text{column dry air} = \frac{\text{column } O_2}{0.2095} \tag{A5}$$

$$= \frac{P_{surf}}{\{g\}_{air} m_{air}^{dry}} - \text{column}_{H_2O} \frac{m_{H_2O}}{m_{air}^{dry}} \tag{A6}$$

where m_{H_2O} is the molecular weight of water ($18.02 \times 10^{-3}/N_A$ kg molecule^{-1}), m_{air}^{dry} is the molecular weight of dry air ($28.964 \times 10^{-3}/N_A$ kg molecule^{-1}), N_A is Avogadro's constant, and $\{g\}_{air}$ is the column-averaged gravitational acceleration.

The TCCON and ACOS-GOSAT algorithms compute the total column of dry air in different ways. Both use a measurement of the O_2 column, but the TCCON approach is to divide the total column of CO_2 by the total column of O_2, measured in the 1.27 µm spectral region (i.e., Eq. A5). This approach is advantageous because the CO_2 and O_2 bands are spectrally close, so many errors caused by instrumental imperfections are reduced in the ratio, and no additional water vapor correction is necessary (Wallace and Livingston, 1990; Yang et al., 2002; Wunch et al., 2011). Mesospheric dayglow from the 1.27 µm O_2 band precludes useful measurements of this band from space, and so the GOSAT instrument measures the O_2 A-band (0.76 µm). The ACOS-GOSAT algorithm cannot simply use the TCCON formulation (Eq. A5) because the A-band is spectrally distant from the CO_2 bands and is measured on a separate detector. Instead, it uses the O_2 A-band measurements to compute a surface pressure, which is then used to compute the dry air column via Eq. (A6), explicitly correcting for the water column with the retrieved value from the ACOS algorithm.

The retrieved X_{CO_2}, denoted $\hat{c}$, can also be described as the profile-weighted column-average CO_2 mixing ratio in dry air, and is related to the retrieved profile, $\hat{x}$, via the pressure weighting function $\boldsymbol{h}$, described by Connor et al. (2008):

$$\hat{c} = \boldsymbol{h}^T \hat{x} \tag{A7}$$

$$= \frac{\text{column } CO_2}{\text{column dry air}} \tag{A8}$$

$$= \frac{\int_0^{P_{surf}} \dfrac{x(p)/(1-f_{H_2O})dp}{g(z(p),\phi)\cdot m_{air}^{dry}\cdot\left[1+f_{H_2O}^{dry}(p)\cdot(m_{H_2O}/m_{air}^{dry})\right]}}{\int_0^{P_{surf}} \dfrac{dp}{g(z(p),\phi)\cdot m_{air}^{dry}\cdot\left[1+f_{H_2O}^{dry}(p)\cdot(m_{H_2O}/m_{air}^{dry})\right]}} \tag{A9}$$

where $x(p)$ is the CO_2 mixing ratio at pressure p, $f_{H_2O}^{dry} \equiv \frac{f_{H_2O}}{1-f_{H_2O}}$, where f_{H_2O} is the atmospheric H_2O abundance, and g is the gravitational acceleration, which is a function of altitude (z) and latitude (ϕ).

The pressure weighting function contains the pressure thicknesses in the state vector, normalized by the surface pressure corrected for the atmospheric H_2O content. Applying $\boldsymbol{h}^T = (h_1, \ldots, h_j, \ldots)$ to both sides of Eq. (A2) gives Eq. (22) in Rodgers and Connor (2003):

$$\hat{c}'_i - c_c = \boldsymbol{h}^T \mathbf{A}_i (\boldsymbol{x} - \boldsymbol{x}_c) + \epsilon_{ci} = \sum_j h_j a_{ij} (\boldsymbol{x} - \boldsymbol{x}_c)_j + \epsilon_{ci}, \tag{A10}$$

where ϵ_{ci} is the measurement error on the column retrieval for instrument i and j is the pressure level. The normalized column averaging kernel is $\boldsymbol{a}_i = (a_{i1}, \ldots, a_{ij}, \ldots)^T$ for instrument i and is defined by Connor et al. (2008), Eq. (8):

$$a_{ij} = \frac{\partial \hat{c}_i}{\partial x_j} \frac{1}{h_j} = \left(\boldsymbol{h}^T \mathbf{A}_i \right)_j \frac{1}{h_j} \tag{A11}$$

The "adjusted" retrieved column $\hat{c}_i'$ is then

$$\hat{c}_i' \equiv \hat{c}_i + \sum_j h_j (\boldsymbol{a}_i - \boldsymbol{u})_j (\boldsymbol{x}_{ai} - \boldsymbol{x}_c)_j \tag{A12}$$

where $\boldsymbol{u}$ is a vector of ones. The difference and variance in the DMFs are then represented by Eqs. (23) and (24) from Rodgers and Connor (2003):

$$\hat{c}_1' - \hat{c}_2' = \sum_j h_j (\boldsymbol{a}_1 - \boldsymbol{a}_2)_j (\boldsymbol{x} - \boldsymbol{x}_c)_j + \epsilon_{c1} + \epsilon_{c2} \tag{A13}$$

$$\sigma^2 (\hat{c}_1' - \hat{c}_2') = \sum_k \sum_j h_j (\boldsymbol{a}_1 - \boldsymbol{a}_2)_j (\boldsymbol{S}_c)_{jk} h_k (\boldsymbol{a}_1 - \boldsymbol{a}_2)_k + \sigma_{c1}^2 + \sigma_{c2}^2 \tag{A14}$$

The matrix $\boldsymbol{S}_c$ is the ensemble covariance matrix, and represents the real atmospheric variability. We will use the convention that GOSAT is $i = 1$, and TCCON is $i = 2$.

For simplicity, we can choose the TCCON a priori profile as the ensemble profile (e.g., $\boldsymbol{x}_{a2} = \boldsymbol{x}_c$). The TCCON a priori profile is a statistically reasonable estimate of X_{CO_2} in the atmosphere – it is an empirical function that is latitude- and time-dependent, built on the GLOBALVIEW data set in the troposphere (GLOBALVIEW-CO$_2$, 2006) and the age-of-air calculations of Andrews et al. (2001) in the stratosphere.

If the first term on the right hand side of Eq. (A14) is small compared with $\sigma_{c1}^2 + \sigma_{c2}^2$, then an adjustment to a common ensemble a priori profile is sufficient to account for the major differences in the two retrievals at the same location and time. This means that we can directly compare $\hat{c}_1'$ and $\hat{c}_2'$.

However, if the first term on the right hand side of Eq. (A14) is not negligibly small, we must reduce our smoothing error by computing what the GOSAT instrument would retrieve given the TCCON total column as "truth," via Eq. (25) from Rodgers and Connor (2003):

$$\hat{c}_{12}' = c_c + \sum_j h_j a_{1j} (\hat{\boldsymbol{x}}_2 - \boldsymbol{x}_c)_j = c_c + \sum_j h_j a_{1j} (\gamma \boldsymbol{x}_c - \boldsymbol{x}_c)_j \tag{A15}$$

Title Page

Abstract | Introduction

Conclusions | References

Tables | Figures

|◄ | ►|

◄ | ►

Back | Close

Full Screen / Esc

Printer-friendly Version

Interactive Discussion

where γ is the TCCON scaling factor applied to the a priori profile to get the final TCCON profile that is then integrated to produce $\hat{c}_2$.

A comparison of $\hat{c}'_{12}$ with $\hat{c}'_1$ (the GOSAT adjusted retrieval) should significantly reduce the smoothing error introduced by the averaging kernels. Analogs of Eqs. (A13) and (A14) for this case are found in Eqs. (26) and (27) of Rodgers and Connor (2003):

$$\hat{c}_1 - \hat{c}_{12} = \sum_j h_j a_{1j} ((\mathbf{I} - \mathbf{A}_2)(\mathbf{x} - \mathbf{x}_c))_j + \epsilon_{c1} - \sum_j h_j a_{1j} \epsilon_{x2j} \tag{A16}$$

$$\sigma^2(\hat{c}_1 - \hat{c}_{12}) = \sum_k \sum_j h_j a_{1j} \left((\mathbf{I} - \mathbf{A}_2) \mathbf{S}_c (\mathbf{I} - \mathbf{A}_2)^T \right)_{jk} h_k a_{1k} + \sigma^2_{c1}$$

$$+ \sum_k \sum_j h_j a_{1j} (\mathbf{S}_{x2})_{jk} h_k a_{1k} \tag{A17}$$

A full profile (from the surface up to 12 km) was measured by an instrumented aircraft over Lamont on 2 August 2009, which provides an example "true" profile (i.e., $\mathbf{x}$). Using this profile to compute $(\mathbf{a}_1 - \mathbf{a}_2)^T (\mathbf{x} - \mathbf{x}_c)$ yields a difference of about 0.2 ppm, which is very small compared with $\epsilon_1 + \epsilon_2 \approx 2.3$ ppm. Figure 3 shows the profiles and averaging kernels used in the calculation above.

Title Page

Abstract | Introduction

Conclusions | References

Tables | Figures

|◄ | ►|

◄ | ►

Back | Close

Full Screen / Esc

Printer-friendly Version

Interactive Discussion

References

Abrams, M., Toon, G., and Schindler, R.: Practical example of the correction of Fourier-transform spectra for detector nonlinearity, Appl. Optics, 33, 6307–6314, 1994. 20910

ACOS-GOSAT Data Access: http://disc.sci.gsfc.nasa.gov/acdisc/data-holdings/acos-data-holdings, last access July 2011. 20904

Andrews, A., Boering, K., Daube, B., Wofsy, S., Loewenstein, M., Jost, H., Podolske, J., Webster, C., Herman, R., Scott, D., Flesch, G. J., Moyer, E. J., Elkins, J. W., Dutton, G. S., Hurst, D. F., Moore, F. L., Ray, E. A., Romashkin, P. A., and Strahan, S. E.: Mean ages of stratospheric air derived from in situ observations of CO_2, CH_4, and N_2O, J. Geophys. Res.-Atmos., 106, 32295–32314, 2001. 20920

Boesch, H., Toon, G., Sen, B., Washenfelder, R., Wennberg, P., Buchwitz, M., De Beek, R., Burrows, J., Crisp, D., Christi, M., Connor, B. J., Natraj, V., and Yung, Y. L.: Space-based near-infrared CO2 measurements: Testing the Orbiting Carbon Observatory retrieval algorithm and validation concept using SCIAMACHY observations over Park Falls, Wisconsin, J. Geophys. Res., 111, 0148–0227, 2006. 20903

Boesch, H., Baker, D., Connor, B., Crisp, D., and Miller, C.: Global Characterization of CO2

Column Retrievals from Shortwave-Infrared Satellite Observations of the Orbiting Carbon Observatory-2 Mission, Remote Sensing, 3, 270–304, doi:10.3390/rs3020270, http://www.mdpi.com/2072-4292/3/2/270/, 2011. 20903

Burrows, J. P., Hölzle, E., Goede, A. P. H., Visser, H., and Fricke, W.: SCIAMACHY–scanning imaging absorption spectrometer for atmospheric chartography, Acta Astronautica, 35, 445–451, doi:10.1016/0094-5765(94)00278-T, http://www.sciencedirect.com/science/article/pii/009457659400278T, earth Observation, 1995. 20917

Butz, A., Guerlet, S., Hasekamp, O., Schepers, D., Galli, A., Aben, I., Frankenberg, C., Hartmann, J.-M., Tran, H., Kuze, A., Keppel-Aleks, G., Toon, G., Wunch, D., Wennberg, P., Deutscher, N., Griffith, D., Macatangay, R., Messerschmidt, J., Notholt, J., and Warneke, T.: Toward accurate CO_2 and CH_4 observations from GOSAT, Geophys. Res. Lett., in press, 2011. 20910

Connor, B., Boesch, H., Toon, G., Sen, B., Miller, C., and Crisp, D.: Orbiting Carbon Observatory: Inverse method and prospective error analysis, J. Geophys. Res., 113, D05305, doi:10.1029/2006JD008336, 2008. 20903, 20919

Conway, T. and Tans, P.: NOAA/ESRL, www.esrl.noaa.gov/gmd/ccgg/trends/, accessed 1 June 2011. 20907

Deutscher, N. M., Griffith, D. W. T., Bryant, G. W., Wennberg, P. O., Toon, G. C., Washenfelder, R. A., Keppel-Aleks, G., Wunch, D., Yavin, Y., Allen, N. T., Blavier, J.-F., Jiménez, R., Daube, B. C., Bright, A. V., Matross, D. M., Wofsy, S. C., and Park, S.: Total column CO_2 measurements at Darwin, Australia – site description and calibration against in situ aircraft profiles, Atmos. Meas. Tech., 3, 947–958, doi:10.5194/amt-3-947-2010, 2010. 20903, 20910

Efron, B. and Gong, G.: A Leisurely Look at the Bootstrap, the Jackknife, and Cross-Validation, The American Statistician, 37, pp. 36–48, http://www.jstor.org/stable/2685844, 1983. 20909

Frankenberg, C., Butz, A., and Toon, G. C.: Disentangling chlorophyll fluorescence from atmospheric scattering effects in O2A-band spectra of reflected sun-light, Geophys. Res. Lett., 38, L03801, doi:10.1029/2010GL045896, 2011. 20910

GLOBALVIEW-CO_2: Cooperative Atmospheric Data Integration Project – Carbon Dioxide, CD-ROM, NOAA GMD, Boulder, Colorado, 2006. 20906, 20908, 20920

Hamazaki, T., Kaneko, Y., Kuze, A., and Kondo, K.: Fourier transform spectrometer for greenhouse gases observing satellite (GOSAT), in: Proceedings of SPIE, vol. 5659, p. 73, 2005. 20901

Hartmann, J.-M., Tran, H., and Toon, G. C.: Influence of line mixing on the retrievals of atmo-

spheric CO_2 from spectra in the 1.6 and 2.1 µm regions, Atmos. Chem. Phys., 9, 7303–7312, doi:10.5194/acp-9-7303-2009, 2009. 20904, 20910

Joiner, J., Yoshida, Y., Vasilkov, A. P., Yoshida, Y., Corp, L. A., and Middleton, E. M.: First observations of global and seasonal terrestrial chlorophyll fluorescence from space, Biogeo-
sciences, 8, 637–651, doi:10.5194/bg-8-637-2011, 2011. 20910

Kalnay, E., Kanamitsu, M., Kistler, R., Collins, W., Deaven, D., Gandin, L., Iredell, M., Saha, S., White, G., Woollen, J., Zhu, Y., Leetmaa, A., Reynolds, B., Chelliah, M., Ebisuzaki, W., Higgins, W., Janowiak, J., Mo, K. C., Ropelewski, C., Wang, J., Jenne, R., and Joseph, D.: The NCEP/NCAR 40-year reanalysis project, B. Am. Meteorol. Soc., 77, 437–471, 1996.
20914

Keppel-Aleks, G., Wennberg, P. O., and Schneider, T.: Sources of variations in total column carbon dioxide, Atmos. Chem. Phys., 11, 3581–3593, doi:10.5194/acp-11-3581-2011, 2011. 20902, 20913

Long, D., Havey, D., Okumura, M., Miller, C., and Hodges, J.: O_2 A-band line parameters to
support atmospheric remote sensing, J. Quant. Spectr. Radiat. T., 111, 2021–2036, 2010. 20904

Messerschmidt, J., Geibel, M. C., Blumenstock, T., Chen, H., Deutscher, N. M., Engel, A., Feist, D. G., Gerbig, C., Gisi, M., Hase, F., Katrynski, K., Kolle, O., Lavrič, J. V., Notholt, J., Palm, M., Ramonet, M., Rettinger, M., Schmidt, M., Sussmann, R., Toon, G. C., Truong,
F., Warneke, T., Wennberg, P. O., Wunch, D., and Xueref-Remy, I.: Calibration of TCCON column-averaged CO_2: the first aircraft campaign over European TCCON sites, Atmos. Chem. Phys. Discuss., 11, 14541–14582, doi:10.5194/acpd-11-14541-2011, 2011. 20903

Morino, I., Uchino, O., Inoue, M., Yoshida, Y., Yokota, T., Wennberg, P. O., Toon, G. C., Wunch, D., Roehl, C. M., Notholt, J., Warneke, T., Messerschmidt, J., Griffith, D. W. T., Deutscher,
N. M., Sherlock, V., Connor, B., Robinson, J., Sussmann, R., and Rettinger, M.: Prelimi-
nary validation of column-averaged volume mixing ratios of carbon dioxide and methane re-
trieved from GOSAT short-wavelength infrared spectra, Atmos. Meas. Tech., 4, 1061–1076, doi:10.5194/amt-4-1061-2011, 2011. 20901

Natraj, V. and Spurr, R.: A fast linearized pseudo-spherical two orders of scattering model to
account for polarization in vertically inhomogeneous scattering-absorbing media, J. Quant. Spectr. Radiat. T., 107, 263–293, 2007. 20904

O'Brien, D., Polonsky, I., O'Dell, C., and Cardehen, A.: Orbiting Carbon Observatory (OCO) al-
gorithm theoretical basis document: The OCO simulator, Cooperative Institute for Research

ACOS-GOSAT X_{CO_2} evaluation with TCCON

D. Wunch et al.

Title Page

Abstract	Introduction
Conclusions	References
Tables	Figures

◄◄	►►
◄	►
Back	Close

Full Screen / Esc

Printer-friendly Version

Interactive Discussion

in the Atmosphere, Colorado State University, Tech. Rep. ISSN, pp. 0737–5352, 2009. 20909

O'Dell, C.: Acceleration of multiple-scattering, hyperspectral radiative transfer calculations via low-streams interpolation, J. Geophys. Res., 115, D10206, doi:10.1029/2009JD012803, 2010. 20904

5 Olsen, S. and Randerson, J.: Differences between surface and column atmospheric CO_2 and implications for carbon cycle research, J. Geophys. Res., 109, D02301, doi:10.1029/2003JD003968, 2004. 20906

Peters, W., Jacobson, A., Sweeney, C., Andrews, A., Conway, T., Masarie, K., Miller, J., Bruhwiler, L., Pétron, G., Hirsch, A., Worthy, D. E. J., van der Werf, G. R., Randerson, J. T.,

10 Wennberg, P. O., Krol, M. C., and Tans, P. P.: An atmospheric perspective on North American carbon dioxide exchange: CarbonTracker, Proc. Natl. Acad. Sci., 104, 18925–18930, 2007. 20916

Rodgers, C.: Inverse methods for atmospheric sounding: Theory and practice, World Scientific Singapore, 2000. 20904

15 Rodgers, C. and Connor, B.: Intercomparison of remote sounding instruments, J. Geophys. Res, 108, 4116–4229, 2003. 20911, 20917, 20919, 20920, 20921

Rothman, L., Gordon, I., Barbe, A., Benner, D., Bernath, P., Birk, M., Boudon, V., Brown, L., Campargue, A., Champion, J., Chance, K., Coudert, L. H., Dana, V., Devi, V. M., Fally, S., Flaud, J.-M., Gamache, R. R., Goldman, A., Jacquemart, D., Kleiner, I., Lacome, N., Lafferty,

20 W. J., Mandin, J.-Y., Massie, S. T., Mikhailenko, S. N., Miller, C. E., Moazzen-Ahmadi, N., Naumenko, O. V., Nikitin, A. V., Orphal, J., Perevalov, V. I., Perrin, A., Predoi-Cross, A., Rinsland, C. P., Rotger, M., Šimečková, M., Smith, M. A. H., Sung, K., Tashkun, S. A., Tennyson, J., Toth, R. A., Vandaele, A. C., and Vander Auwera, J.: The HITRAN 2008 molecular spectroscopic database, J. Quant. Spectr. Radiat. T., 110, 533–572, 2009. 20904

25 Savtchenko, A. and Avis, C.: README Document for ACOS Level 2 Standard Product, http://disc.sci.gsfc.nasa.gov/acdisc/documentation/ACOS.shtml, 2010. 20904

Spurr, R.: Simultaneous derivation of intensities and weighting functions in a general pseudo-spherical discrete ordinate radiative transfer treatment, J. Quant. Spectr. Radiat. T., 75, 129–175, 2002. 20904

30 Spurr, R., Kurosu, T., and Chance, K.: A linearized discrete ordinate radiative transfer model for atmospheric remote-sensing retrieval, J. Quant. Spectr. Radiat. T., 68, 689–735, 2001. 20904

Suto, H. and Kuze, A.: Correction of scan-speed instability of TANSO-FTS on GOSAT, Abstract

ACOS-GOSAT X$_{CO_2}$ evaluation with TCCON

D. Wunch et al.

A51C-0107 presented at 2010 Fall Meeting, AGU, San Francisco, Calif., 13–17 December 2010. 20905

Tanaka, T., et al.: The 2010 Aircraft Calibration Campaign over Tsukuba, Japan, in preparation, 2011. 20913

5 Toth, R., Brown, L., Miller, C., Malathy Devi, V., and Benner, D.: Spectroscopic database of CO_2 line parameters: 4300–7000 cm^{-1}, J. Quant. Spectr. Radiat. T., 109, 906–921, 2008. 20904

Tran, H. and Hartmann, J.: An improved O_2 A band absorption model and its consequences for retrievals of photon paths and surface pressures, J. Geophys. Res., 113, D18104, doi:10.1029/2008JD010011, 2008. 20904

10 Wallace, L. and Livingston, W.: Spectroscopic observations of atmospheric trace gases over Kitt Peak. I – Carbon dioxide and methane from 1979 to 1985, J. Geophys. Res., 95, 9823–9827, doi:10.1029/JD095iD07p09823, 1990. 20918

Washenfelder, R., Toon, G., Blavier, J., Yang, Z., Allen, N., Wennberg, P., Vay, S., Matross, D., and Daube, B.: Carbon dioxide column abundances at the Wisconsin Tall Tower site, J.
15 Geophys. Res., 111, D22305, doi:10.1029/2006JD007154, 2006. 20903

Wofsy, S. C., Daube, B. C., Jimenez, R., Kort, E., Pittman, J. V., Park, S., Commane, R., Xiang, B., Santoni, G., Jacob, D., Fisher, J., Pickett-Heaps, C., Wang, H., Wecht, K., Wang, Q.-Q., Stephens, B. B., Schertz, S., Romashkin, P., Campos, T., Haggerty, J., Cooper, W. A., Rogers, D., Beaton, S., Elkins, J. W., Fahey, D., Gao, R., Moore, F., Montzka, S. A., Schwartz,
20 J. P., Hurst, D., Miller, B., Sweeney, C., Oltmans, S., Nance, D., Hintsa, E., Dutton, G., Watts, L. A., Spackman, R., Rosenlof, K., Ray, E., Zondlo, M., Diao, M., Mahoney, M. J., Chahine, M., Olsen, E., Keeling, R., Bent, J., Atlas, E. A., Lueb, R., Patra, P., Ishijima, K., Engelen, R., Nassar, R., Jones, D. B., and Mikaloff-Fletcher, S.: HIAPER Pole-to-Pole Observations (HIPPO): Fine grained, global scale measurements for determining rates for
25 transport, surface emissions, and removal of climatically important atmospheric gases and aerosols, Phil. Trans. R. Soc. A, 369, 2073–2086, doi:10.1098/rsta.2010.0313, 2011. 20906

Wunch, D., Toon, G. C., Wennberg, P. O., Wofsy, S. C., Stephens, B. B., Fischer, M. L., Uchino, O., Abshire, J. B., Bernath, P., Biraud, S. C., Blavier, J.-F. L., Boone, C., Bowman, K. P., Browell, E. V., Campos, T., Connor, B. J., Daube, B. C., Deutscher, N. M., Diao, M., Elkins,
30 J. W., Gerbig, C., Gottlieb, E., Griffith, D. W. T., Hurst, D. F., Jiménez, R., Keppel-Aleks, G., Kort, E. A., Macatangay, R., Machida, T., Matsueda, H., Moore, F., Morino, I., Park, S., Robinson, J., Roehl, C. M., Sawa, Y., Sherlock, V., Sweeney, C., Tanaka, T., and Zondlo, M. A.: Calibration of the Total Carbon Column Observing Network using aircraft profile data,

Atmos. Meas. Tech., 3, 1351–1362, doi:10.5194/amt-3-1351-2010, 2010. 20903

Wunch, D., Toon, G. C., Blavier, J.-F. L., Washenfelder, R., Notholt, J., Connor, B. J., Griffith, D. W. T., Sherlock, V., and Wennberg, P. O.: The Total Carbon Column Observing Network, Phil. Trans. R. Soc. A, 369, 2087–2112, doi:10.1098/rsta.2010.0240, 2011. 20902, 20903, 20910, 20918

Yang, Z., Toon, G., Margolis, J., and Wennberg, P.: Atmospheric CO_2 retrieved from ground-based near IR solar spectra, Geophys. Res. Lett., 29, 53–1, 2002. 20918

Yang, Z., Wennberg, P., Cageao, R., Pongetti, T., Toon, G., and Sander, S.: Ground-based photon path measurements from solar absorption spectra of the O_2 A-band, J. Quant. Spectr. Radiat. T., 90, 309–321, 2005. 20910

Yokota, T., Oguma, H., Morino, I., and Inoue, G.: A nadir looking SWIR FTS to monitor CO_2 column density for Japanese GOSAT project, Proc. Twenty-fourth Int. Sympo. on Space Technol. and Sci.(Selected Papers), pp. 887–889, 2004. 20901

York, D., Evensen, N., Martínez, M., and Delgado, J.: Unified equations for the slope, intercept, and standard errors of the best straight line, American Journal of Physics, 72, 367–375, doi:10.1119/1.1632486, 2004. 20914

Title Page

Abstract | Introduction

Conclusions | References

Tables | Figures

⏮ | ⏭

◄ | ►

Back | Close

Full Screen / Esc

Printer-friendly Version

Interactive Discussion

Table 1. Filters applied to the ACOS v2.8 data. The filters that differ from the master quality flag are the χ^2 filter cut-off values, the surface pressure filter and the aerosol optical depth filter. (The quantity f_{year} is the fractional year (i.e., 2009.4). The first GOSAT measurements were recorded on 2009.26.) The additional filters that are not included in the master quality flag are listed below the line. The aerosol optical depth is measured at 0.755 µm.

Filter	Filter criterion
Retain data with good spectral fits	reduced_chi_squared_o2_fph $< 1.2 + 0.088 \times (f_{year} - 2009.26)$
	reduced_chi_squared_strong_co2_fph $< 1.2 + 0.040 \times (f_{year} - 2009.26)$
	reduced_chi_squared_weak_co2_fph $< 1.2 + 0.064 \times (f_{year} - 2009.26)$
Retain data with well-retrieved surface elevation	$|(\Delta P) - \overline{\Delta P}| < 5$ hPa
	(ΔP = surface_pressure_fph − surface_pressure_apriori_fph)
Retain scenes without extreme aerosol optical depth values	$0.05 <$ retrieved_aerosol_aod_by_type < 0.15
	(use the first of the 5 rows of the matrix)
Retain data with no diverging steps	diverging_steps = 0
Retain scenes with no cloud	cloud_flag = 0
Retain data that converge	outcome_flag = 1 or 2
Retain data with 'H' gain only	gain_flag = 'H'
Retain no glint data	glint_flag = 0
Retain scenes without cloud over ice	2.4×albedo_o2_fph − 1.13×albedo_strong_co2_fph < 1
Retain scenes unless with nonzero X$_{CO_2}$ uncertainties	xco2_uncert $\neq 0$

Title Page

Abstract | Introduction

Conclusions | References

Tables | Figures

◄◄ | ►►

◄ | ►

Back | Close

Full Screen / Esc

Printer-friendly Version

Interactive Discussion

Table 2. Parameters and values for Eq. (4). The coefficients list the values for three assumptions of the X_{CO_2} field in the Southern Hemisphere: 1, that there is a small seasonal cycle and a 1.89 ppm/year secular increase (i.e., Eq. 4); 2, that there is only a 1.89 ppm yr^{-1} secular increase (i.e., no seasonal cycle); and 3, that there is a small seasonal cycle, a 1.89 ppm yr^{-1} secular increase, and a -1 ppm gradient between 25° S and 55° S. The errors are twice the bootstrapped standard errors. The coefficients have units of ppm/unit of blended albedo, ppm/hPa, ppm/airmass and ppm/(10^7 W cm^{-2} sr^{-1} (cm^{-1})$^{-1}$), respectively.

Parameter	Mean value	Coefficients		
		Assumption 1	Assumption 2	Assumption 3
blended_albedo	0.3	10.5 ± 0.4	10.2 ± 0.4	10.1 ± 0.4
ΔP	10.9 hPa	-0.15 ± 0.01	-0.14 ± 0.01	-0.16 ± 0.01
airmass	2.6	-2.0 ± 0.4	-2.2 ± 0.4	-2.1 ± 0.4
signal_o2	3.4×10^{-7} W cm^{-2} sr^{-1} (cm^{-1})$^{-1}$	-0.25 ± 0.08	-0.23 ± 0.08	-0.24 ± 0.08
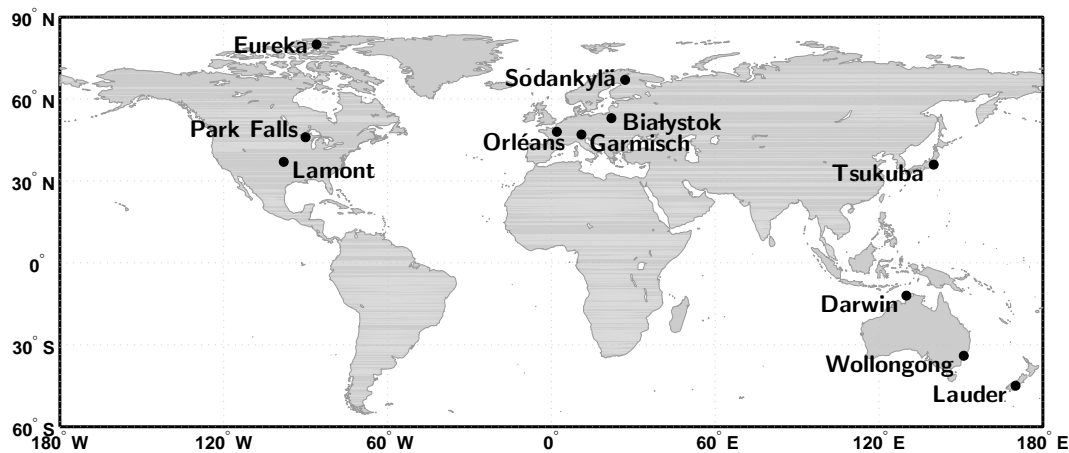
Fig. 1. The locations of the TCCON stations used in this study.
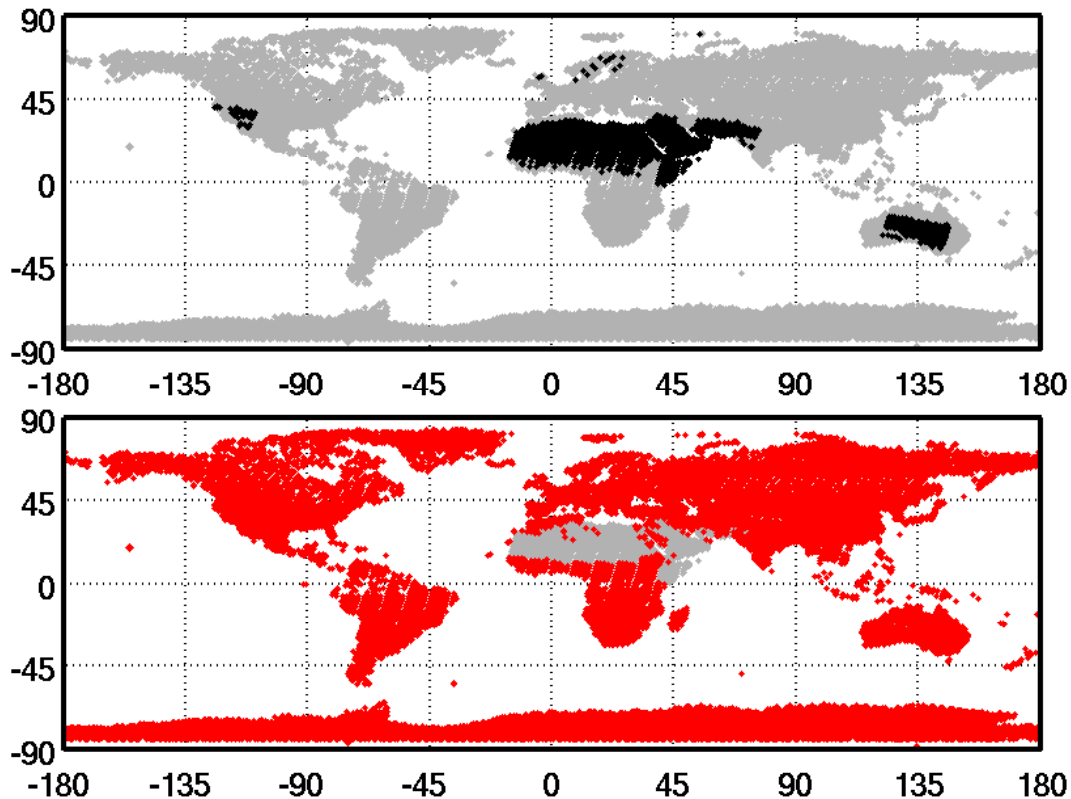
Fig. 2. Masking out desert or bright regions of the Earth which use M gain. The grey points represent all of the ACOS-GOSAT soundings over land from 5 April 2009 through 21 March 2011. Overlaid are all M-gain points (top panel, black), and H-gain points (bottom panel, red). All red points are kept; all black points are removed.

Title Page

Abstract | Introduction

Conclusions | References

Tables | Figures

|◄ | ►|

◄ | ►

Back | Close

Full Screen / Esc

Printer-friendly Version

Interactive Discussion
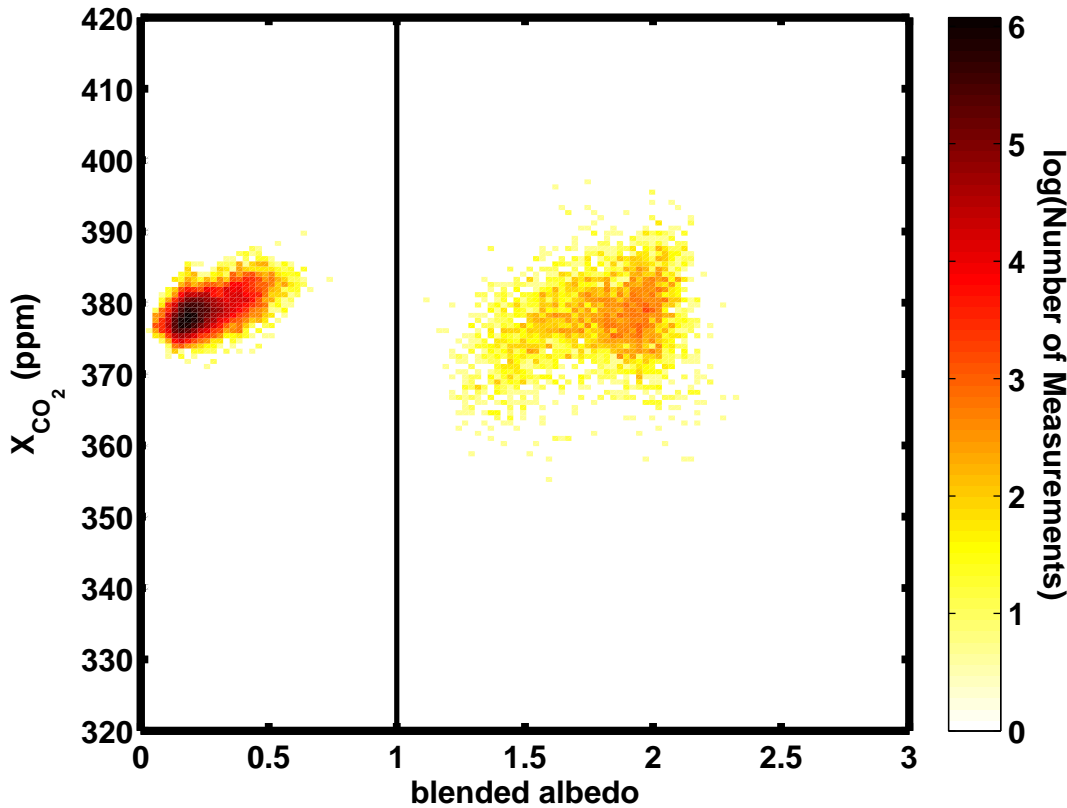
Fig. 3. An illustration of how snowy or icy scenes affect the ACOS-GOSAT data. There are two clear populations of points, delineated by a value of 1 in blended albedo (defined in Eq. 2 of the main text). Points to the left of the line at 1 are not influenced by snow and ice, and they are retained; points to the right are discarded. The colours represent the logarithm of the number of measurements in each 0.7 ppm by 0.025 units of blended albedo.

Full Screen / Esc

Printer-friendly Version

Interactive Discussion
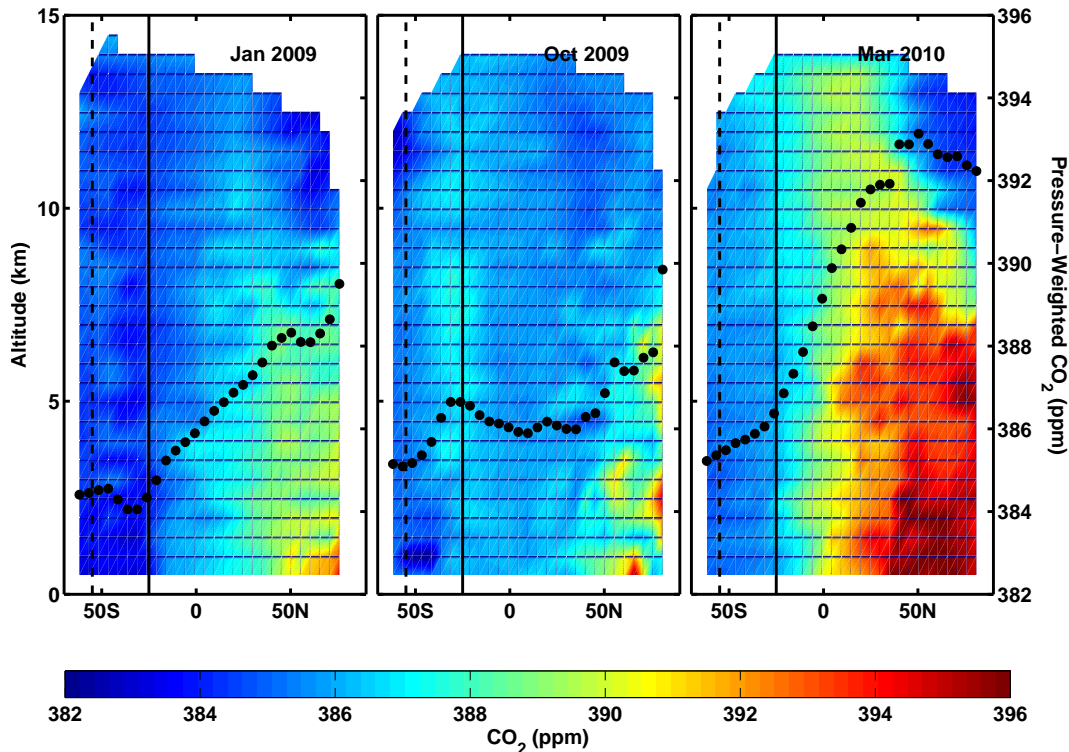
Fig. 4. Three slices of the atmospheric CO_2 are plotted for the three HIPPO flights at different times of the year. There is generally smaller variability in the Southern Hemisphere south of 25° S (indicated by the solid vertical black line) than in the Northern Hemisphere. 99.9 % of the filtered ACOS-GOSAT data in the Southern Hemisphere south of 25° S lie between 25° S and 55° S (indicated by the dashed vertical black line). The black circles are the pressure-weighted mean mixing ratios at each 5-degree latitude bin, with their values on the right axis. Note that the black circles are not total column amounts, and will be affected by missing data in the stratosphere.

Title Page

Abstract | Introduction

Conclusions | References

Tables | Figures

|◄ | ►|

◄ | ►

Back | Close

Full Screen / Esc

Printer-friendly Version

Interactive Discussion
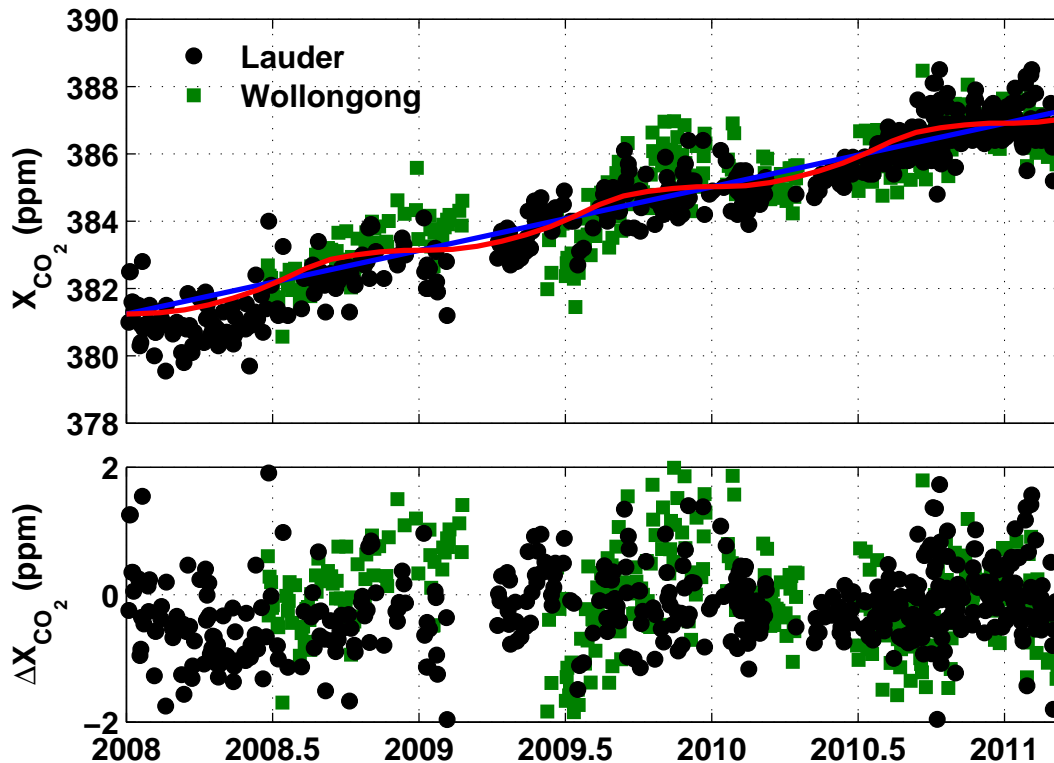
Fig. 5. The time series of the Southern Hemisphere TCCON data from Lauder, New Zealand and Wollongong, Australia are plotted in the top panel, along with the 1.89 ppm yr^{-1} secular increase (blue). The Baring Head GLOBALVIEW climatological seasonal cycle with a time lag of 6 weeks and a reduced amplitude ($\times 0.65$) is superimposed on the secular increase (red). In the bottom panel, the red curve is removed from the Lauder and Wollongong data to show the residuals.

Fig. 6. The black curve is the original, unmodified ACOS-GOSAT data between 25° S and 55° S in both panels. The global bias (0.982) between the ACOS-GOSAT and TCCON data is removed in the left panel to obtain the yellow curve, and Eq. (4) is applied to obtain the red curve in the right panel. The grey shading represents 1σ. The TCCON data from Lauder, New Zealand (black circles) and Wollongong, Australia (green circles) are plotted for comparison.
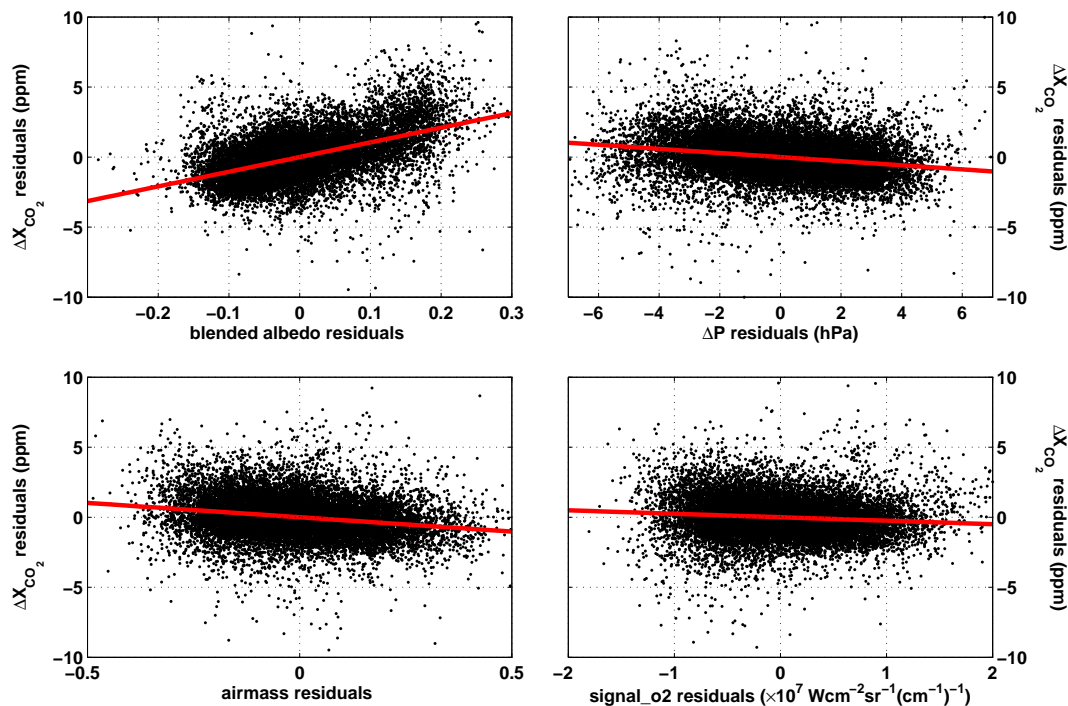
Fig. 7. A scatter plot showing the relationship between ΔX_{CO_2} and the parameters simultaneously fitted in Eq. (4). These are data only from the Southern Hemisphere, where there should be no significant X_{CO_2} variations. The black dots show the adjusted data, the solid red lines are the best fit lines described by the coefficients listed in Table 2.

Full Screen / Esc

Printer-friendly Version

Interactive Discussion
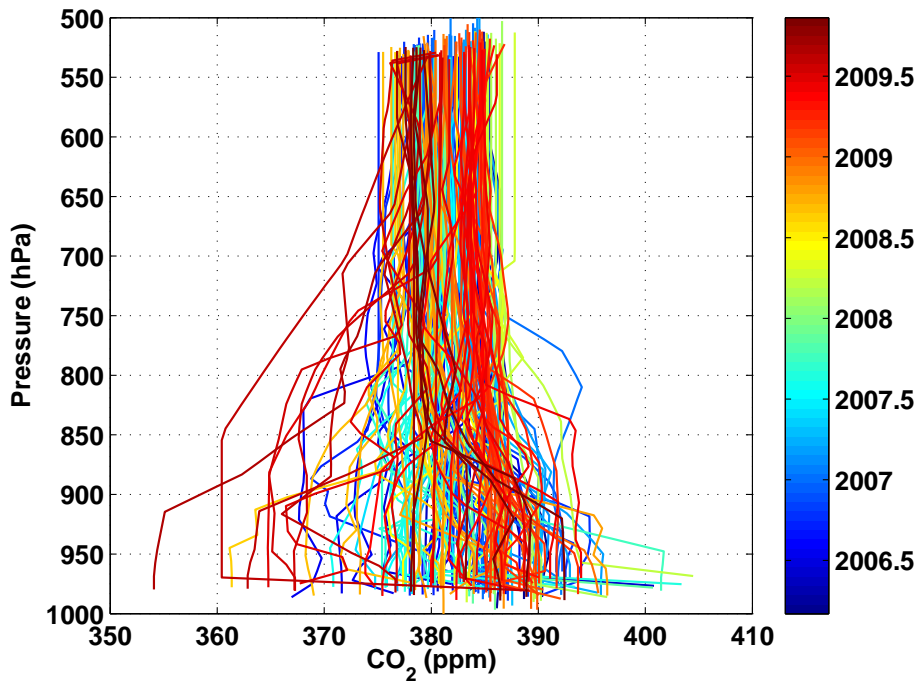
Fig. 8. All the Cessna profiles over Lamont, OK, are shown on a pressure grid, coloured by the time the profile was measured. These profiles are detrended to show only the seasonality and variability.
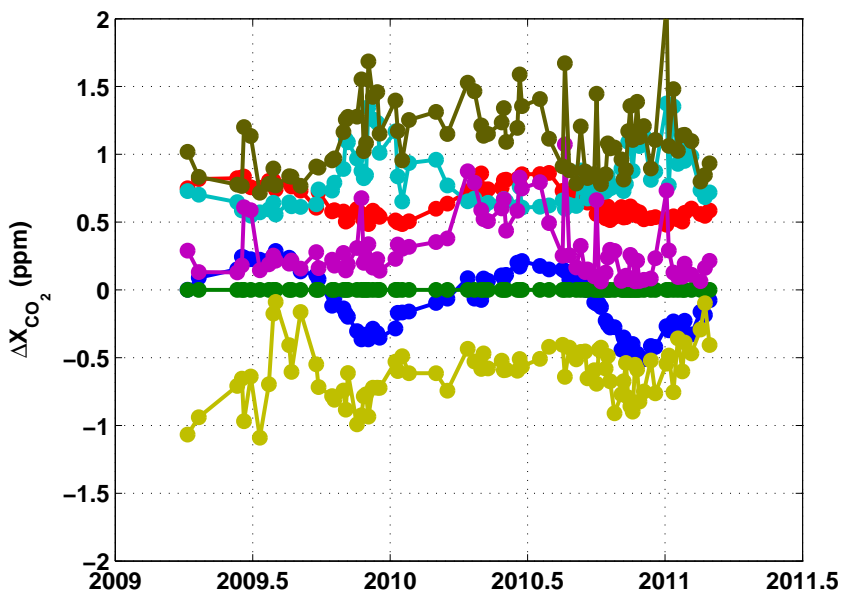
Fig. 9. The curves in this figure show the effect of the choice of a priori profile, and the effect of smoothing by the averaging kernels for data measured over the Lamont TCCON site. Plots show the ACOS-GOSAT adjustment to the ensemble profile ($(a_1 - u)^T(x_{a1} - x_c)$, blue), the TCCON adjustment to the ensemble profile ($(a_2 - u)^T(x_{a2} - x_c) = 0$, green), the smoothing error ($(a_1 - a_2)^T S_c (a_1 - a_2)$, red), the ACOS-GOSAT variance (XCO2_Var, σ_1^2, cyan), the TCCON variance (σ_2^2, purple), the difference between the TCCON adjusted ACOS-GOSAT smoothed values ($\hat{c}'_{12} - \hat{c}'_2$, yellow) and the sum of the TCCON and ACOS-GOSAT variances ($\sigma_1^2 + \sigma_2^2$, dark green). All parameters are defined in the Appendix.

Title Page

Abstract | Introduction

Conclusions | References

Tables | Figures

|◄ | ►|

◄ | ►

Back | Close

Full Screen / Esc

Printer-friendly Version

Interactive Discussion
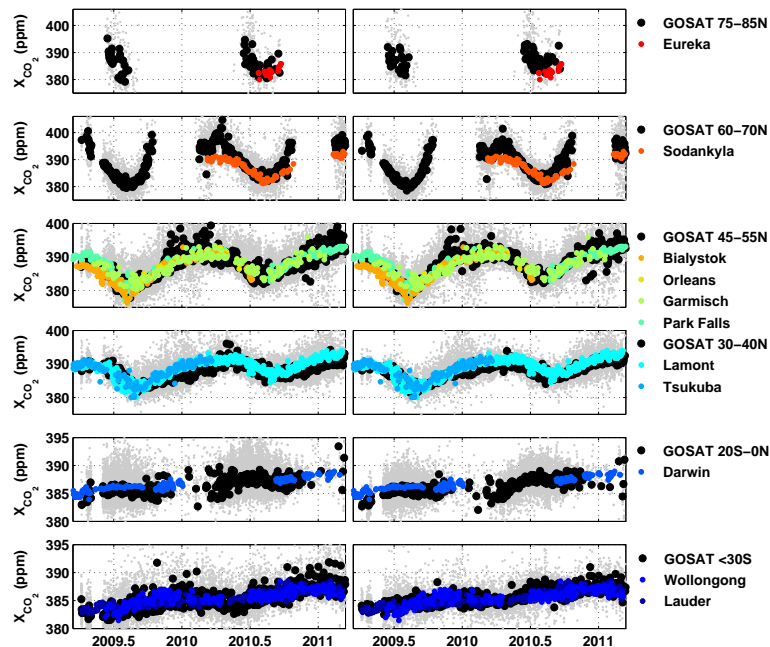
Fig. 10. Seasonal-cycle comparisons. These panels show the ACOS-GOSAT data adjusted by only the global bias (0.982, left panels) and after applying Eq. (4) (right panels). Each row of panels shows a different latitude range for the ACOS-GOSAT data (the black circles are the daily median zonal average values, and the grey dots are the individual measurements), and the TCCON daily median data within the latitude band (multi-coloured circles). The agreement and variability in the ACOS-GOSAT data are visibly improved in the right-hand panels.

Full Screen / Esc

Printer-friendly Version

Interactive Discussion
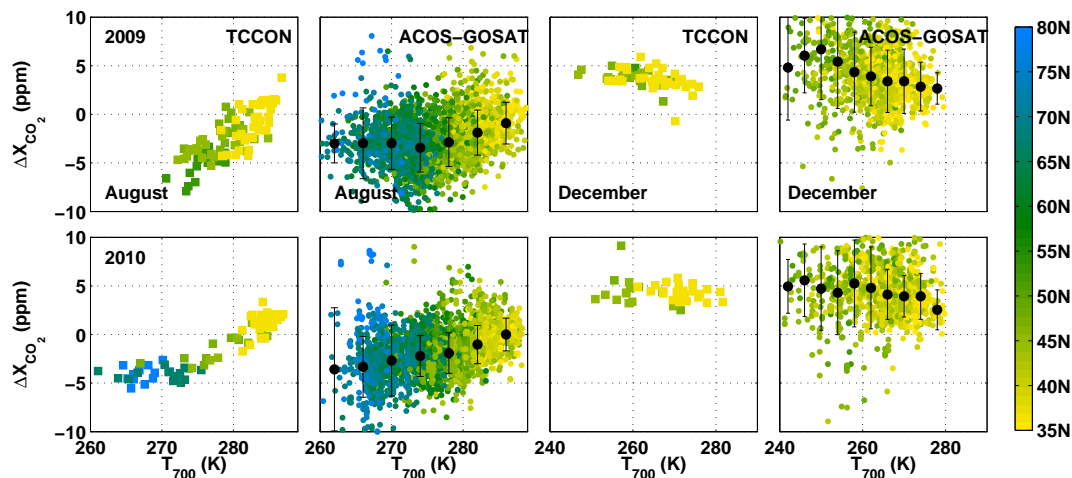
Fig. 11. Plotted here are X_{CO_2} anomalies against the temperature at 700 hPa. The anomalies are computed by subtracting a 1.89 ppm yr^{-1} secular increase from the X_{CO_2} time series. There is a strong positive relationship in the summertime, and this relationship reverses in sign in the winter. The top row of panels shows data from 2009, and the bottom row shows data from 2010. The first two columns of panels contain data from August, and the right two columns show December. The TCCON data are plotted in squares; the modified ACOS-GOSAT data are circles, and the medians and standard deviations of the ACOS-GOSAT data at each 2 K bin are plotted in black circles with error bars. The colours represent the latitude. Although there are no TCCON data at the highest latitudes (lowest T_{700}) in 2009, the TCCON sites operating in both years show a visibly stronger drawdown (indicated by more negative ΔX_{CO_2}) in the August 2009 than in the 2010 TCCON data. This is indistinguishable within the standard deviation of the ACOS-GOSAT data. The ACOS-GOSAT data nicely capture the reversal in sign of the X_{CO_2}-T_{700} slope in the winter.

Title Page

Abstract | Introduction

Conclusions | References

Tables | Figures

|◄ | ►|

◄ | ►

Back | Close

Full Screen / Esc

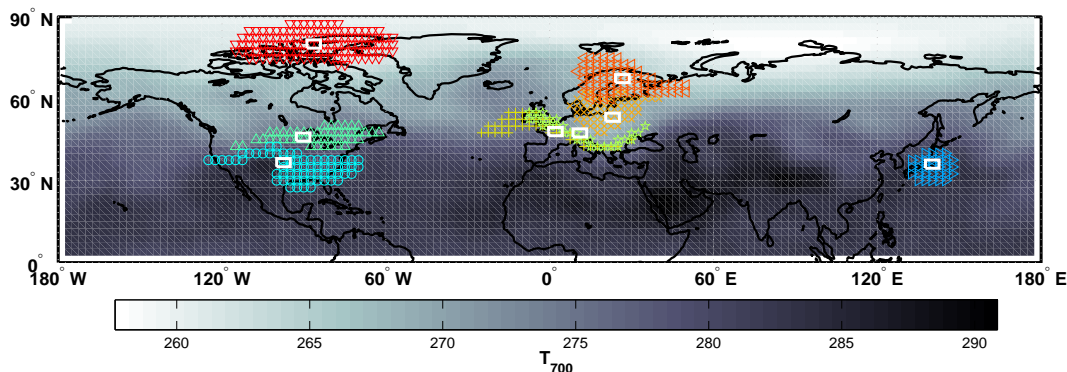Printer-friendly Version

Interactive Discussion

Fig. 12. A map of the coincidence criteria for a ten-day period in August, 2010. The background T_{700} field is from the NCEP/NCAR analysis. The white boxes show the $\pm0.5°$ latitude and $\pm1.5°$ longitude limits about each TCCON site. The symbols in colour show the locations on the Earth for this ten-day period that satisfy the coincidence criteria that T_{700} is within ±2 K, latitude is within $\pm10°$, and longitude is within $\pm30°$. (The only exception to this is the Tsukuba site, where the longitude criterion is tightened to $\pm10°$ to avoid over-weighting data over China.) The actual locations of the coincidences with the ACOS-GOSAT data would be restricted to the regions overlaid in colour, where the ACOS-GOSAT data exist (i.e., only over land and in cloud-free scenes).

Title Page

Abstract · Introduction

Conclusions · References

Tables · Figures

⏮ · ⏭

◀ · ▶

Back · Close

Full Screen / Esc

Printer-friendly Version
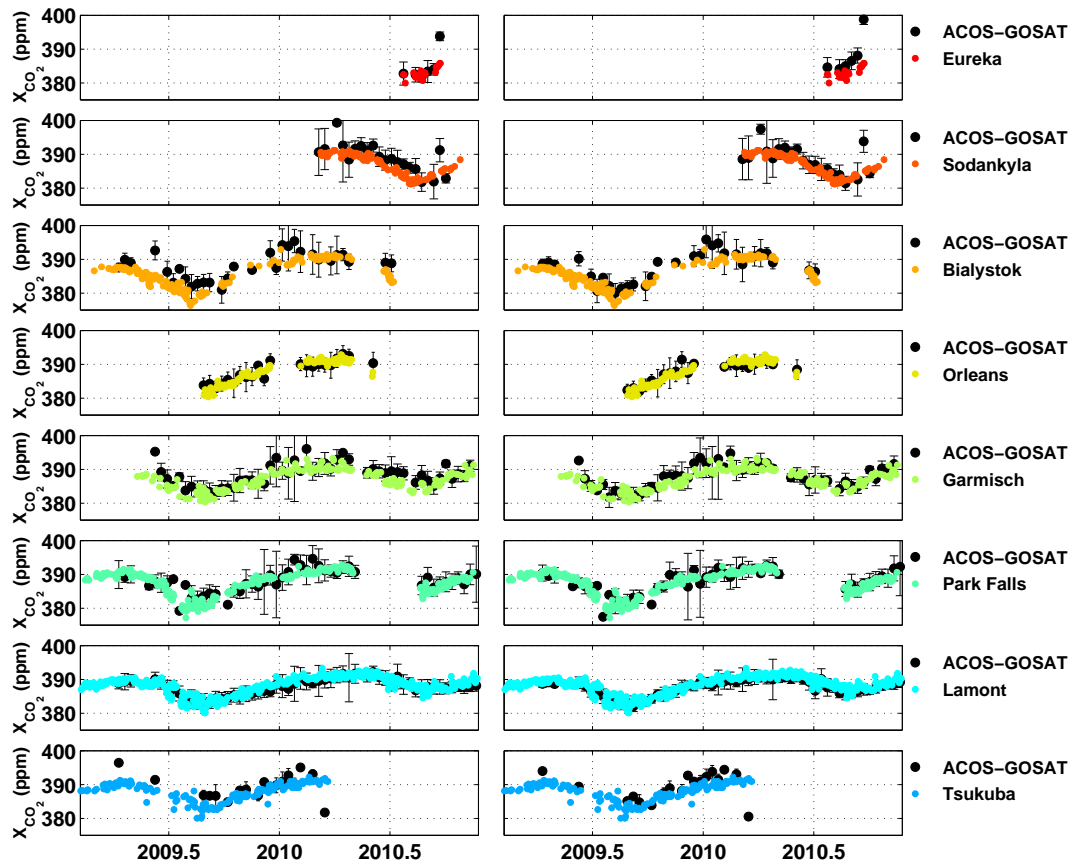
Interactive Discussion

Fig. 13. A site-by-site comparison between ACOS-GOSAT and the Northern Hemisphere TC-CON sites, using the T_{700} coincidence criterion. The left panel shows the ACOS-GOSAT data after applying the global bias (0.982), and the right panel shows the data after applying Eq. (4).

Title Page

Abstract | Introduction

Conclusions | References

Tables | Figures

◄◄ | ►►

◄ | ►

Back | Close

Full Screen / Esc

Printer-friendly Version

Interactive Discussion
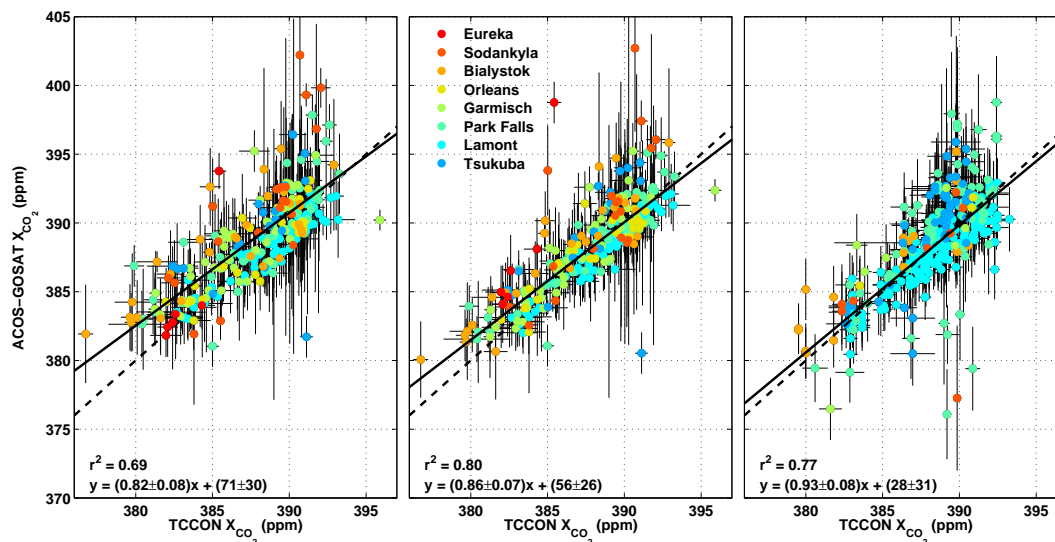
Fig. 14. The left two panels show the correlation between TCCON and ACOS-GOSAT using the T_{700} coincidence criterion. The left panel shows the large-scale bias-corrected, but otherwise unmodified, data. The middle panel shows the correlation after applying Eq. (4). The right-hand panel shows the correlation after applying Eq. (4), but using coincidence criteria that restricts latitudes to within ±0.5°, longitudes to within ±1.5°, and interpolates the TCCON data onto the ACOS-GOSAT measurement times. Note that there are no coincident data over Eureka when using the geographic coincidence criteria (right-hand panel). The solid lines show the best fit to the data (with equations shown on the plot), and the one-to-one line is plotted as a dashed line. The quoted errors are 2σ.

Title Page

Abstract | Introduction

Conclusions | References

Tables | Figures

|◄ | ►|

◄ | ►

Back | Close

Full Screen / Esc
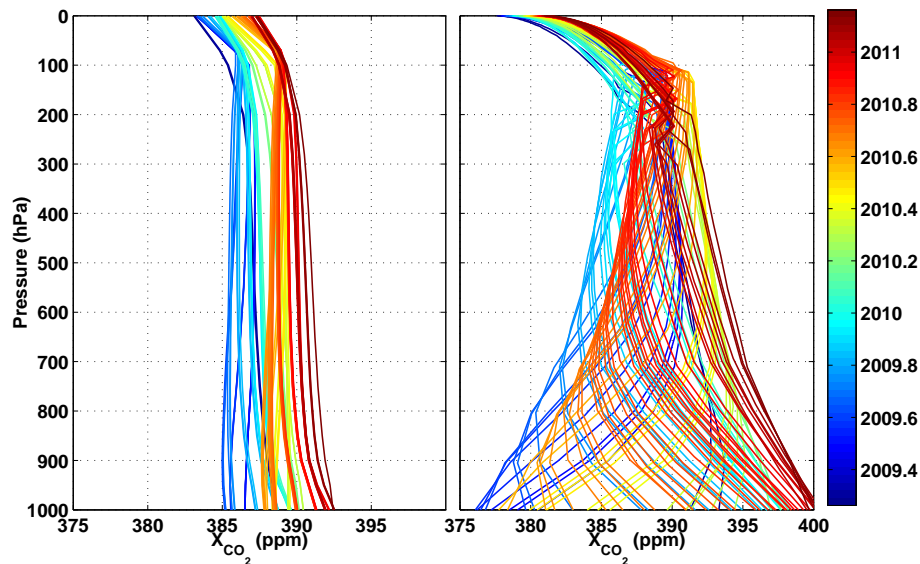
Printer-friendly Version

Interactive Discussion

Fig. A1. A priori profiles at the Lamont TCCON site for ACOS-GOSAT (left panel) and TCCON (right panel), coloured by the year.

Title Page

Abstract | Introduction

Conclusions | References

Tables | Figures

|◄ | ►|

◄ | ►

Back | Close

Full Screen / Esc
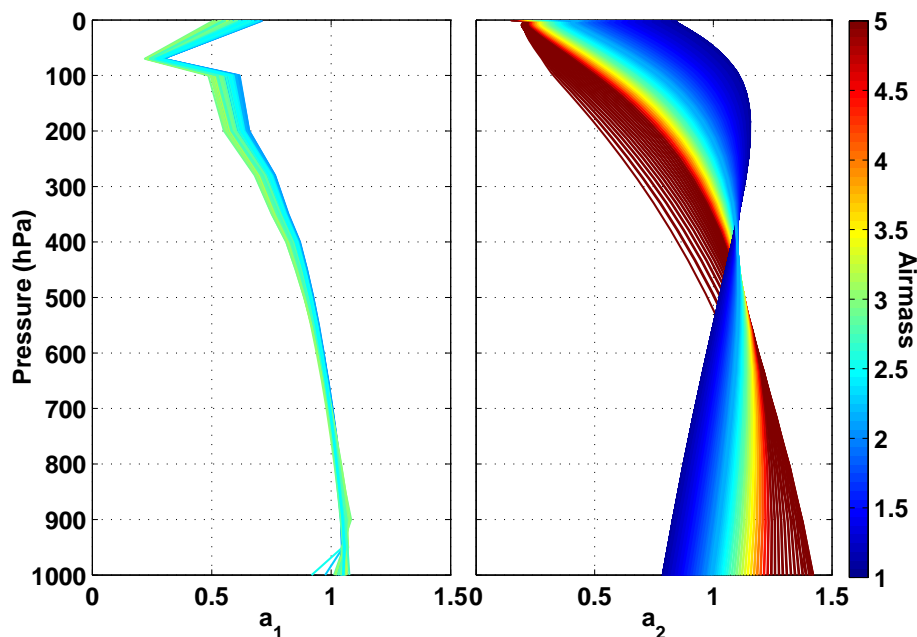
Printer-friendly Version

Interactive Discussion

Fig. A2. Column averaging kernels for ACOS-GOSAT (left panel) and TCCON (right panel), coloured by the airmass. The GOSAT airmass range plotted here is much smaller than the range of TCCON airmasses.
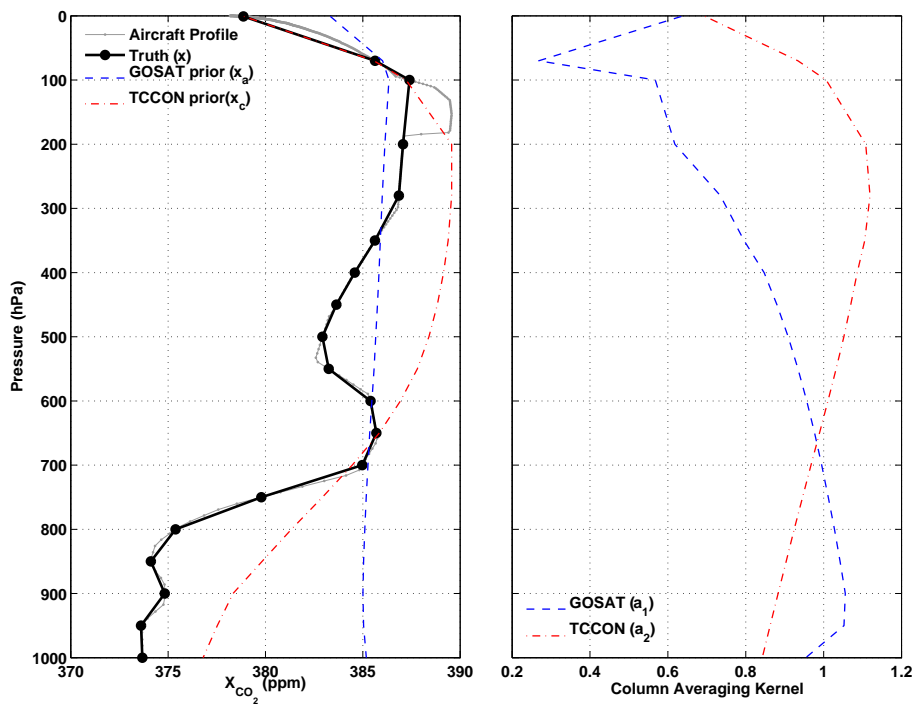
Fig. A3. Plots from 2 August 2009, when there was an overflight of Lamont that spanned a large altitude range (0–12 km). The left panel shows the aircraft profile (grey) which uses the TCCON a priori profile to fill in the stratosphere above the aircraft ceiling, the true profile (black; i.e., the aircraft profile interpolated onto the ACOS retrieval grid), the ACOS-GOSAT a priori profile (blue) and the TCCON a priori profile (red). The right panel shows the ACOS-GOSAT (blue) and TCCON (red) column averaging kernels for the time of the aircraft measurement.